Supplementary Information for

Biosynthesis of polybrominated aromatic organic compounds by marine bacteria

Vinayak Agarwal, Abrahim A. El Gamal, Kazuya Yamanaka, Dennis Poth, Roland D. Kersten, Michelle Schorn, Eric E. Allen, Bradley S. Moore

SUPPLEMENTARY RESULTS

Supplementary Note 1

Detection of dehydrogenation and halogenation of L-proline acylated to Bmp1.

Trypsin-digested N-His_6-Bmp1(ACP) was analyzed by LC-MS/MS. 10 µL of the trypsin-digested assay mixture was injected onto a reverse phase C_4 column (Vydac 5 µm, 4.6 mm × 250 mm). Water + 0.1% formic acid was used as solvent A, and MeCN + 0.1% formic acid was used as solvent B. The elution profile was as follows (0.7 mL/min): 10% B for 10 min, linear increase to 30% B across 5 min, linear increase to 70% B across 40 min, linear decrease to 10% B across 5 min, linear increase to 100% B across 1 min followed by 2 min at 100% B, decrease to 10% B across 1 min, 10% B for 2 min and 5 min of post-time equilibration. The assay relies on the detection of MS2 product ions **i–v** as shown in **Supplementary Fig. 7**. Briefly, ion **i** would be generated by collision-induced disassociation for holo-N-His_6-Bmp1(ACP) and ion **ii** by pyrrolyl-*S*-N-His_6-Bmp1(ACP). Ions **iii–v** correspond to brominated variants for phosphopantetheinylated halo-pyrrole ions as previously described in the literature[1-2]. Expression of N-His_6-Bmp1(ACP) in *E.* coli should provide a mixture of apo-N-His_6-Bmp1(ACP), and holo-N-His_6-Bmp1(ACP) as a result of crosstalk with fatty acid biosynthesis. The side chain hydroxyl of the serine residue at the carboxy terminus of the α-2 helix for the Bmp1(ACP) should be post-translationally esterified with phosphopantetheine for holo-N-His_6-Bmp1(ACP), but not for apo-N-His_6-Bmp1(ACP). By sequence homology, this serine residue was identified to be Ser35 for Bmp1. Holo-N-His_6-Bmp1(ACP) will not participate further in the assay, as acylation by Sfp (*B. subtilis* phosphopantetheinyl transferase) requires the presence of a non-esterified Ser35 side chain. The presence of holo-N-His_6-Bmp1(ACP) was confirmed by detection of MS2 ion **i**. As a second means of independent verification, the MS2 ion **i** was traced back to a MS1

peptide fragment of N-His_6-Bmp1(ACP) that bears the Ser35 residue. For peptide mapping, the mass of the holo-peptide fragment was calculated based on the mass of the monoisotopic peak for the peptide, and its charge state (z). For calculation of the mass of the apo-peptide fragment, the mass corresponding to ion **vi** was subtracted from it. The mass of the apo-peptide fragment thus determined could be traced to the peptide fragment generated by trypsin digestion of His_6-Bmp1(ACP) as shown in **Fig. 3** and **Supplementary Fig. 8**. The equations for calculation of the apo-peptide fragment mass corresponding to holo-N-His_6-Bmp1(ACP) as identified in **Supplementary Fig. 8** are as follows:

$$z = 1/(mass\ difference\ between\ successive\ isotope\ peaks)$$

$$apo\ peptide\ mass = [(parent\ ion\ \times z) - (z\ \times 1.00728)] - 340.0858$$

Upon transfer of **16** to apo-N-His_6-Bmp1(ACP), MS2 ion **ii** could be detected, and upon mono- di-, and tri-halogenation by Bmp2, ejection ions corresponding to **iii–v** could be detected. The apo-peptide fragments generating these MS2 ions were mapped back to Bmp1(ACP) by subtraction of the mass of ions **viii–x** (**Supplementary Fig. 7**) from the respective holo-peptide masses.

Using this assay methodology, we could generate N-His_6-pyrrolyl-*S*-Bmp1(ACP) by loading **16** onto the apo-N-His_6-Bmp1(ACP). Upon addition of Bmp2, SsuE (*E. coli* flavin reductase), NADPH and KBr, mono-, di-, and tri-brominated Bmp1(ACP) peptides could be detected, thus establishing tri-bromination of the pyrrole ring by Bmp2. No halogenation was observed when KBr was replaced with KCl or KI. Regiospecificity for bromination of the pyrrole ring by Bmp2 is assumed to be similar to the pyrrole chlorinase PltA due to high sequence similarity between the two enzymes.

Supplementary Note 2

Identification and characterization of polybrominated biphenyl and OH-BDE products generated by Bmp7 *in vitro,* and a mass spectrometry-based detection of OH-BDEs in culture extracts.

MS1 for the Bmp7 *in vitro* reaction analyte (**Supplementary Fig. 20**, panel **a**) led to determination of the molecular weights of different product species, and together with the typical isotopic distribution afforded by bromination, molecular formulae of the products could be discerned. With **4** as a substrate, three isomers each for the molecular formulae $C_{12}H_6O_2Br_4$ (**Supplementary Fig. 20**, panel **b**) and $C_{12}H_7O_2Br_3$ (**Supplementary Fig. 20**, panel **c**) could be reproducibly detected as the major products of the reaction. The most abundant isotope ion for each formula was then selected for targeted MS/MS by collision induced disassociation. An identical approach was used to analyze products of the reaction with 2,4-dichlorophenol (**17**) (described later). The molecular formulae for the major products, $C_{12}H_6O_2Br_4$ and $C_{12}H_7O_2Br_3$, could be putatively assigned to biphenyl products **1** and **10**, respectively, as both molecules have previously been isolated from *Pseudoalteromonas* species. Upon chromatographic analysis of authentic synthetic standards of **1** and **10** (**Supplementary Fig. 19**), we could assign one of the isomers for $C_{12}H_6O_2Br_4$ as **1**, and one of the isomers for $C_{12}H_7O_2Br_3$ as **10**. These assignments were further confirmed by preparative scale purification of these two products from large scale *in vitro* Bmp7 reactions, and comparison of ^{1}H NMR spectra against values reported in literature[3-4]. While the mechanism for synthesis of **1** from **4** is expected to be analogous to bi-radical aryl coupling reactions[5-6], the production of **10** would additionally entail dehalogenation that has been reported in literature for aryl-coupling enzymes employing radical intermediates[7].

MS/MS analysis for **1** and **10** showed $[M\text{-}Br^-]^-$ and $[M\text{-}2Br^-]^-$ MS2 product ions (**Supplementary Fig. 20**, panels **d–e**, and panel **f** respectively), as would be expected for polybrominated biphenyls. Another isomer for $C_{12}H_7O_2Br_3$ also showed $[M\text{-}Br^-]^-$ MS2 product ions (**Supplementary Fig. 20**, panel **f**), leading to its assignment as a biphenyl (denoted by * in **Fig. 5a**). However, the molecule could not be isolated from large-scale Bmp7 reactions in sufficient quantities for comprehensive structure elucidation by NMR spectroscopy. As this species is isomeric with **10**, and is putatively a polybrominated biphenyl, we postulate its structure to be 3,3',5-tribromo-[1,1'-biphenyl]-2,4'-diol.

At this point, the identities of the other two isomers of $C_{12}H_6O_2Br_4$ and one isomer for $C_{12}H_7O_2Br_3$ were unknown. One of the isomers of $C_{12}H_6O_2Br_4$ (retention time ~ 28.2 min) showed MS2 product ions corresponding to dibromobenzoquinone (**Supplementary Fig. 20**, panel **g**). This ion could not be generated by a polybrominated biphenyl species, as scission of the carbon-carbon bond between the two aryl rings would lead to the formation of a dibromophenol ion, regardless of the positions of the bromines on the benzene ring. However, an OH-BDE molecule, in which scission of the ether bond occurs prior to the loss of bromine during MS/MS can generate a MS2 ion corresponding to dibromobenzoquinone as observed in panel **g**, and also reported in literature for para-OH-BDEs[8]. Hence, we putatively assigned this species as a para-OH-BDE. This hypothesis was supported by the observation that an isomeric OH-BDE to **1** should have a greater retention time than **1**, as one of the hydrophilic hydroxyl groups in **1** would be involved in ether bond formation in the OH-BDE. Preparative scale purification of this species from large scale Bmp7 reactions, and structure elucidation by NMR led to assignment of the structure as 2,6-dibromo-4-(2,4-dibromophenoxy)phenol (**11**) (**Supplementary Fig. 21**). Structure assignments for OH-BDEs are based upon ^{1}H NMR, HSQC, HMBC, and H2BC experiments. ^{13}C NMR shifts, deduced from HSQC, HMBC and H2BC correlations, are listed in the figure below. Specifically, **11**

was isolated by preparative HPLC separation of products from ethyl acetate extracts of large scale Bmp7 reactions with **4**. The solvent was removed *in vacuo*, and dried overnight to yield a white residue. The residue was dissolved in d_6-DMSO and NMR spectra collected using 600 MHz Varian NMR microprobe. Deduced structure of the molecule with proton shifts listed in red, and carbon shifts as deduced from HSQC and HMBC couplings listed in green is shown in panel **a** below. HSQC correlations are shown as thick bonds, HMBC correlations are shown as red arrows, and H2BC[11] correlations are shown as blue arrows in panel **b** below.

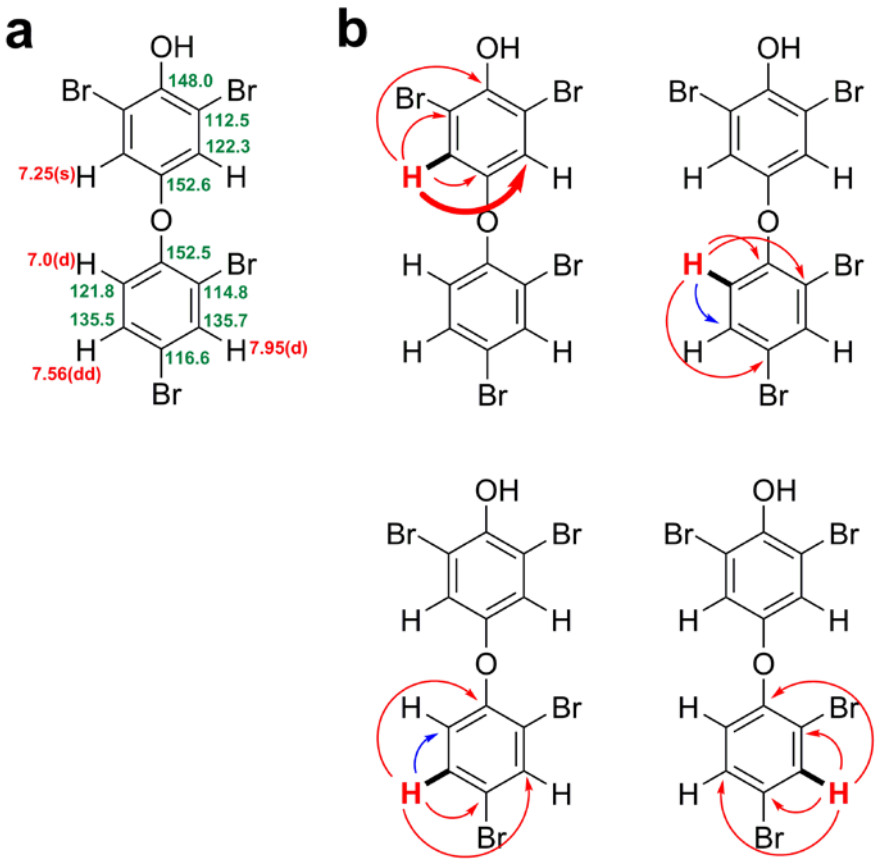

Note that the symmetry of one aryl ring is supported by the presence of a singlet in the ^{1}H NMR (**Supplementary Fig. 21**), and the HMBC coupling shown as a bold arrow that is identical to a HSQC coupling. Symmetry for the aryl rings is also supported by MS/MS fragmentation consistent with para-OH-BDE[8] (**Supplementary Fig. 20**). The isomeric ortho-OH-BDE (2′-OH-BDE-68) would have no symmetrical aryl ring. The ^{1}H and ^{13}C shifts

reported here for the non-symmetrical aryl ring are in agreement with those reported in literature[12].

One of the isomers for $C_{12}H_7O_2Br_3$ exhibiting MS2 product ions corresponding to monobromobenzoquinone (**Supplementary Fig. 20**, panel **h**), was isolated and its structure characterized by NMR spectroscopy to be 2-bromo-4-(2,4-dibromophenoxy)phenol (**12**). Specifically, **12** was isolated by preparative HPLC purification of ethyl acetate extracts of large scale Bmp7 reactions with **4**. The solvent was removed *in vacuo*, and dried overnight to yield a white residue. The residue was dissolved in d_6-DMSO and NMR spectra collected using 600 MHz Varian NMR microprobe. Deduced structure of the molecule with proton shifts listed in red and carbon shifts listed in green is shown panel **a** below. HSQC correlations are shown as thick bonds, HMBC correlations are shown as red arrows, and H2BC[11] correlations are shown as blue arrows in panel **b** below.

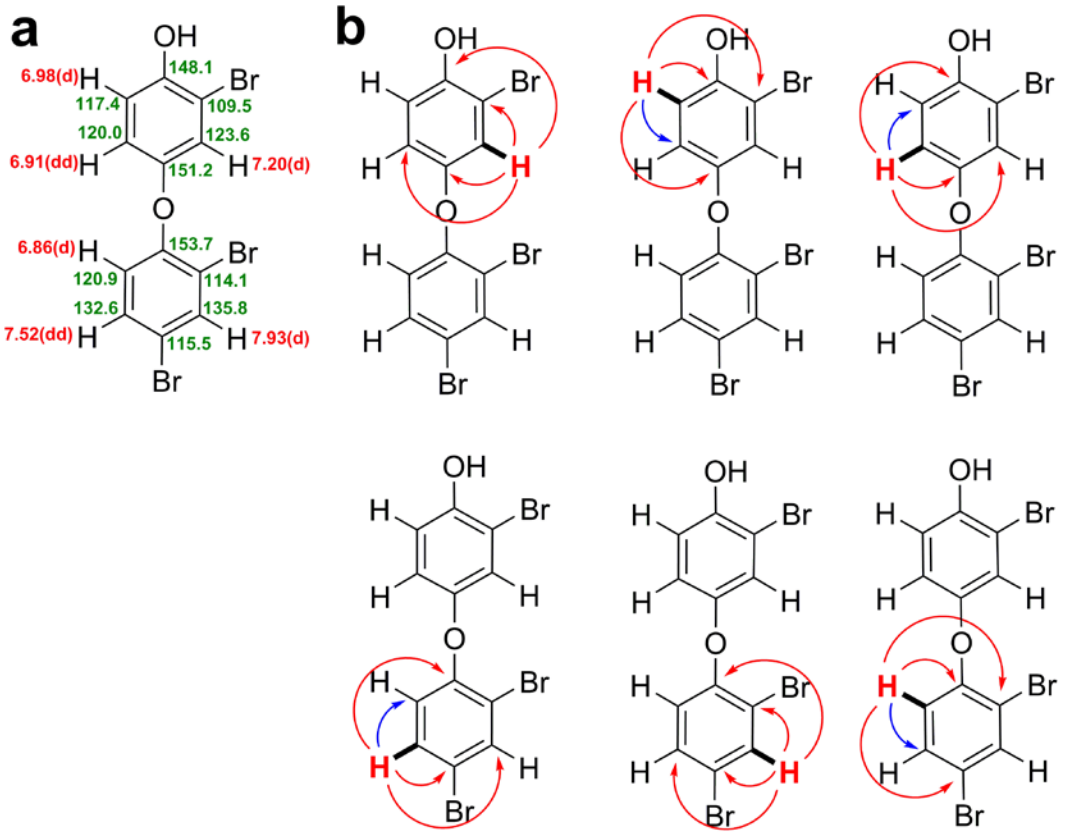

12: ^{1}H NMR (600 MHz, DMSO) δ 7.93 (d, *J* = 2.3 Hz, 1H), 7.52 (dd, *J* = 8.8, 2.4 Hz, 1H), 7.20 (d, *J* = 2.9 Hz, 1H), 6.98 (d, *J* = 8.8 Hz, 1H), 6.91 (dd, *J* = 8.8, 2.8 Hz, 1H), 6.86 (d, *J* = 8.8 Hz, 1H). The ^{1}H and ^{13}C shifts reported here for the aryl ring bearing two bromine atoms are in agreement with those reported in literature[12]. Overall, the NMR assignments are in agreement with previous report of **12** isolated from marine algae[13]. Structure assignment is also supported by MS/MS fragmentation consistent with para-OH-BDE[8] (**Supplementary Fig. 20**).

Hence, as this point, all three isomers for $C_{12}H_7O_2Br_3$ and two isomers for $C_{12}H_6O_2Br_4$ had been identified. Both **11** and **12** are para-OH-BDEs, in that the ether linkage is positioned para to the phenolic hydroxyl. The third, and as yet unidentified isomer for $C_{12}H_6O_2Br_4$, was also postulated to be an OH-BDE due to its higher retention time than **1**, and similar retention time as the OH-BDE **11**. However, this species demonstrated no major MS2 product ions. Envisaging a OH-BDE isomer for **11**, we rationalized the structure for this species to be 2,4-dibromo-6-(2,4-dibromophenoxy)phenol (2'-OH-BDE-68) (**13**). This hypothesis was confirmed by the successive addition of increasing amounts of commercially available synthetic **13** (AccuStandard, HBDE-4006S-CN) to the Bmp7 reaction extracts and by observation of an identical retention time of the Bmp7 reaction product to synthetic **13** standard (**Supplementary Fig. 22**). Hence, by a combination of LC-MS/MS, NMR spectroscopy and comparison to synthetic standards, all major products produced by the Bmp7 reaction could be identified. Notably, **13** is an ortho-OH-BDE, in that the ether linkage resides ortho to the phenolic hydroxyl. Differential MS/MS fragmentation of ortho- and para-OH-BDEs has been reported in literature[8]. The dibromobenzoquinone and monobromobenzoquinone MS2 ions for **11** and **12** respectively were used as signatures to mine the LC-MS/MS data for bacterial extracts, leading to the identification of **11** and **12** in the extracts of producer strains. It should be noted that the culture extracts contained more

than fifteen polybrominated aromatic organic molecules, in addition to other small molecules. This precluded a facile prior identification of OH-BDE molecules, as done for **1–3** from the culture extracts. Additionally, identification of ortho-OH-BDE relies on comparison to authentic synthetic standards as they do not possess a distinct MS/MS signature.

5 did not demonstrate a typical absorbance shift associated with substrate binding for Bmp7 (**Supplementary Fig. 12**). However, as **5** is a product generated by Bmp5 (**Supplementary Fig. 17**) and is present in the Δ*bmp7* extracts (**Supplementary Fig. 5**), we explored whether **5** could be used by Bmp7 as a substrate. Indeed, Bmp7 could use **5**, though substrate consumption was significantly lower as compared to that for **4** (**Supplementary Fig. 23**). A singular major product could be identified, with the MS1 predicted formula $C_{12}H_5Br_5O_2$ (**Supplementary Fig. 24**, panel **a**). As a dibromobenzoquinone MS2 product ion was observed (**Supplementary Fig. 24**, panel **b**), we postulated that the product of the reaction to be a para-OH-BDE. Preparative-scale purification of the product from large scale Bmp7 reactions with **5**, and subsequent NMR characterization led to the identification of the chemical structure of the product as 2,6-dibromo-4-(2,4,6-tribromophenoxy)phenol (**14**). Specifically, **14** was isolated by preparative HPLC separation of products from ethyl acetate extracts of large scale Bmp7 reactions with **5**. The solvent was removed *in vacuo*, and dried overnight to yield a white residue. The residue was dissolved in d_6-DMSO, NMR spectra collected using 600 MHz Varian NMR microprobe. Final deduced structure of the molecule, with the proton shifts listed in red, and the carbon shifts listed in green is shown in panel **a** below. HSQC correlations are shown as thick bonds, HMBC correlations in red arrows are shown in panel **b** below. No H2BC[11] correlations were observed.

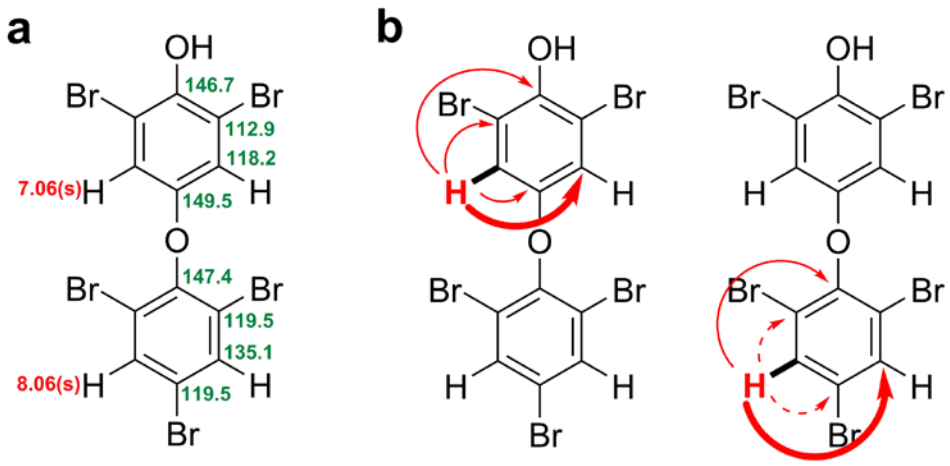

14: ^{1}H NMR (600 MHz, DMSO) δ 8.08 (s, 1H), 7.06 (s, 1H). Uncertainty in the assignment of two HMBC couplings is shown as dashed arrows, and is likely caused by the highly similar ^{13}C shifts of the two carbon atoms in the symmetrical ring. Note that the symmetry of both aryl rings is supported by the presence of only two singlets in the ^{1}H NMR, and the HMBC couplings shown in bold arrows that are identical to HSQC couplings. Symmetry for both rings is also supported by MS/MS fragmentation consistent with para-OH-BDEs[8] (**Supplementary Fig. 24**). A hypothetical isomeric ortho-OH-BDE would have only one symmetrical aryl ring.

Using the above discussion for products generated by Bmp7 using **4** and **5** as substrates, we could rationalize the products generated by Bmp7 using **17** as a substrate (**Supplementary Fig. 25**, panel **a**). It should be noted that **17** is not a physiological product generated by Bmp5 as Bmp5 does not incorporate chloride. LC-MS/MS analysis identifies three major isomeric product peaks with the molecular formula $C_{12}H_6Cl_4O_2$ (**Supplementary Fig. 25**, panel **b**). The first product peak showed $[M\text{-}Cl^-]^-$, $[M\text{-}2Cl^-]^-$, and $[M\text{-}3Cl^-]^-$ MS2 product ions (**Supplementary Fig. 25**, panels **c**, **d** and **e**, respectively). This lead to the assignment of this species as 4,4',6,6'-tetrachloro-2,2'-biphenol (**18**), a chlorinated analog of **1**. The second isomeric product peak demonstrated MS2 product ions corresponding to

dichlorobenzoquinone (**Supplementary Fig. 25**, panel **f**), leading to a putative assignment of its structure as 2,6-dichloro-4-(2,4-dichlorophenoxy)phenol (**19**). The third isomeric product did not show any major MS2 product ions. By analogy to Bmp7 brominated products, the structure for this species can be postulated to be 2,4-dichloro-6-(2,4-dichlorophenoxy)phenol (20). Though **18–20** are not as yet reported natural products, several million tons of **17** are industrially synthesized each year, and also generated by the degradation of the herbicide 2,4-dichlorophenoxyacetic acid. Hence, it is conceivable that **17** could exist in the marine microbial metabolome, owing to anthropogenic origins, or enzymatically synthesized by homologs of the Bmp5 enzymes. Consequently, **18–20**, and other reaction products of Bmp7 with **17** may already exist as halogenated marine natural products.

Supplementary Figures

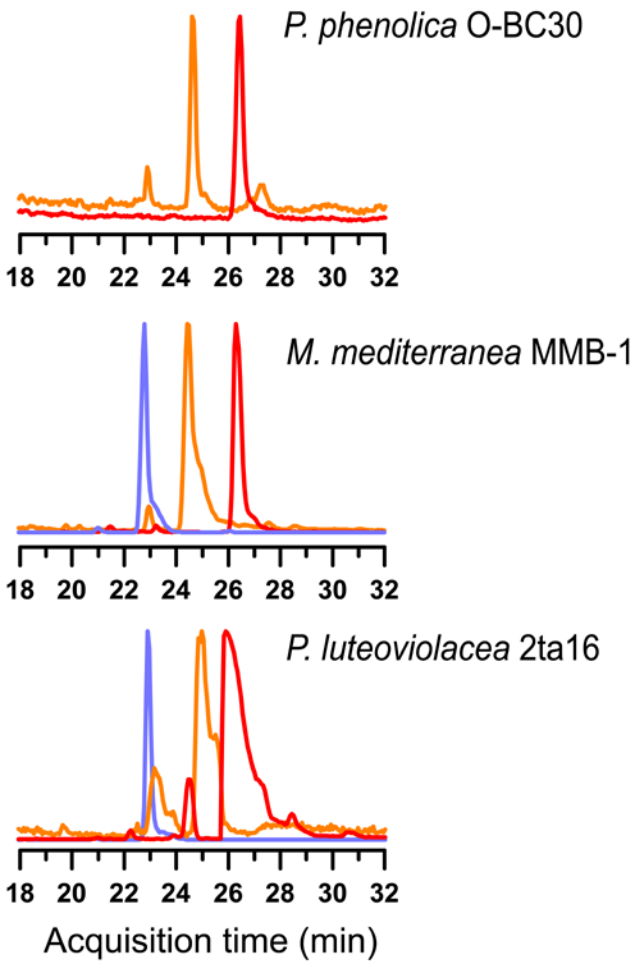

Supplementary Fig. 1. Production of signature polybrominated molecules 1–3 by marine bacteria. Extracted ion chromatograms (EICs) for extracts of *P. luteoviolacea* 2ta16, *P. phenolica* O-BC30, and *M. mediterranea* MMB-1 analyzed by LC-MS/MS demonstrating the production of **1** (red curves), **2** (violet curves), and **3** (orange curves). Bacteria were grown in Difco 2216 Marine Broth without additional supplementation of bromide. Extracts dissolved in MeOH were injected onto a reverse phase C_{18} column (Phenomenex Luna , 5 µm, 4.6 × 100 mm) operating on an Agilent 1260 HPLC in tandem to an Agilent 6530 Accurate Mass Q-TOF mass spectrometer. The solvents used for HPLC were water + 0.1% formic acid (A) and MeCN + 0.1% formic acid (B). The HPLC elution profile was as follows (flow rate 0.5 mL/min): 10% B for 5 min, linear gradient to 70% B across 10 min, linear increase to 100% B across 30 min, 100% B for 3 min, linear decrease to 10% B across 2 min, 10% B for 5 min. An identical LC-MS/MS profile has been used for all analytical scale heterologous culture extract analysis, Bmp7 reaction extracts, and for synthetic standards.

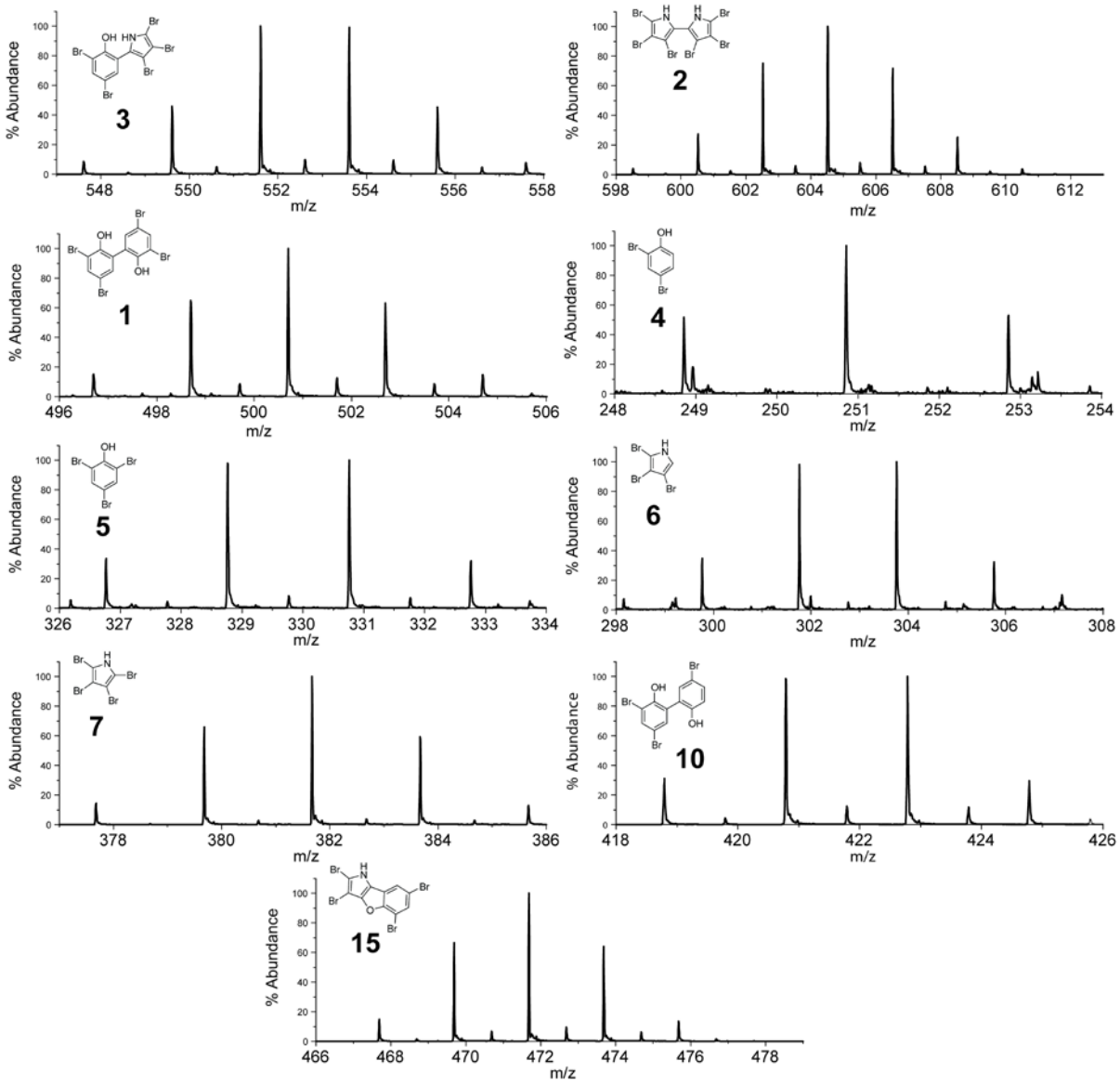

Supplementary Fig. 2. High-resolution mass spectra for selected polybrominated metabolites from an organic extract of *P. luteoviolacea* 2ta16. For accurate mass determination, an organic extract of *P. luteoviolacea* 2ta16 was analyzed by LC-ESI-MS in negative polarity on an Agilent 6230 Accurate Mass TOF-MS at the UCSD Chemistry and Biochemistry Molecular Mass Facility (La Jolla, CA). Isotope patterns for **1–7**, **10** and **15** identified in the culture extract of *P. luteoviolacea* 2ta16 are shown. See also **Supplementary Table 1** for error estimation in mass spectra.

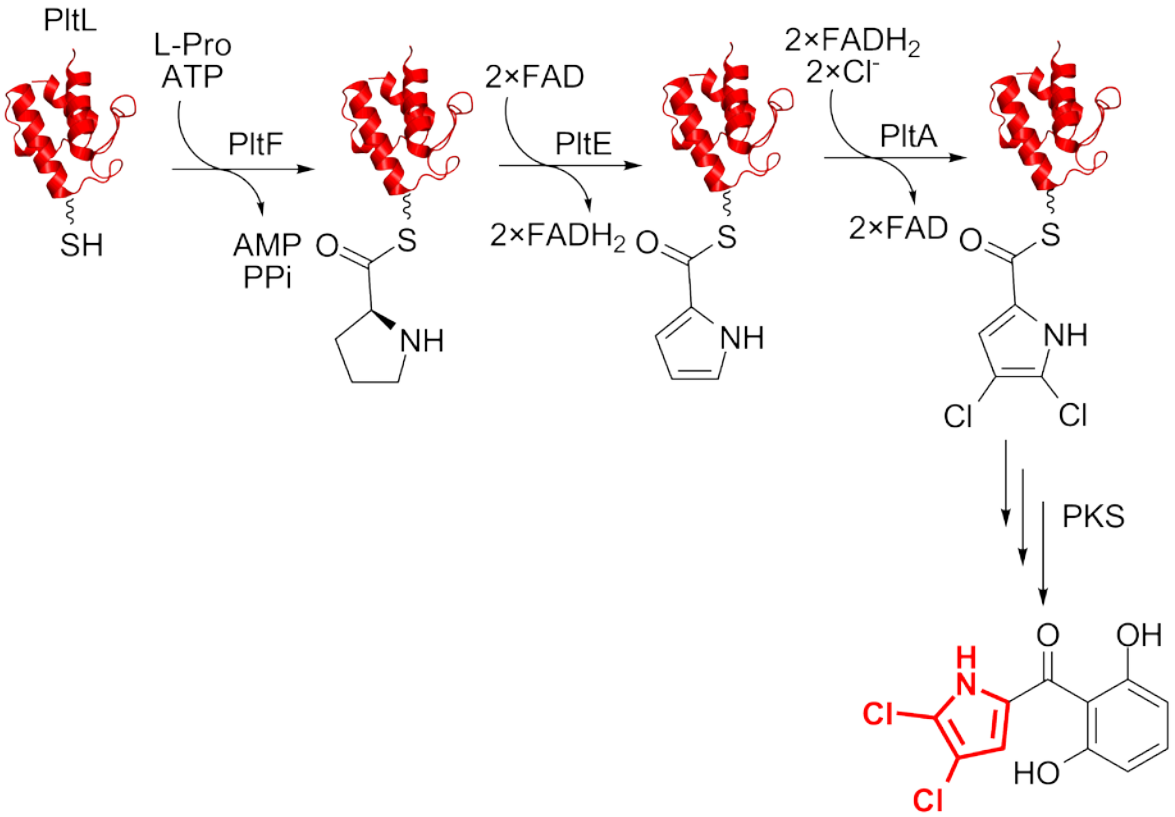

Supplementary Fig. 3. Chemical logic for the biosynthesis of halogenated pyrrole moieties in natural products. The scheme for the generation of dichlorinated pyrroles, tethered to an ACP molecule is shown as characterized for pyoluteorin biosynthesis[1,27]. The ACP (PltL) is phosphopantetheinylated to yield a free sulfhydryl moiety, which is then acylated to an amino acid (L-proline) by virtue of a thioester bond by an adenyltransferase PltF. This reaction requires the hydrolysis of a stoichiometric amount of ATP to AMP and PP_i. Subsequent to acylation, the pyrrolidine ring is dehydrogenated by PltE, with concomitant reduction of two FAD molecules to $FADH_2$. The pyrrole ring is then dichlorinated by the chlorinase PltA (5-position followed by 4-position). Halogenation requires reduced flavin cofactor, and appropriate halide ion in the presence of molecular oxygen. In the pyoluteorin biosynthetic scheme, the dichlorinated pyrrolyl-*S*-ACP then undergoes three rounds of polyketide extension, and subsequent release and aromatization. The dichlorinated pyrrole moiety in pyoluteorin is highlighted in red. The canonical four helix-bundle architecture of ACP (PltL) is shown in the red cartoon.

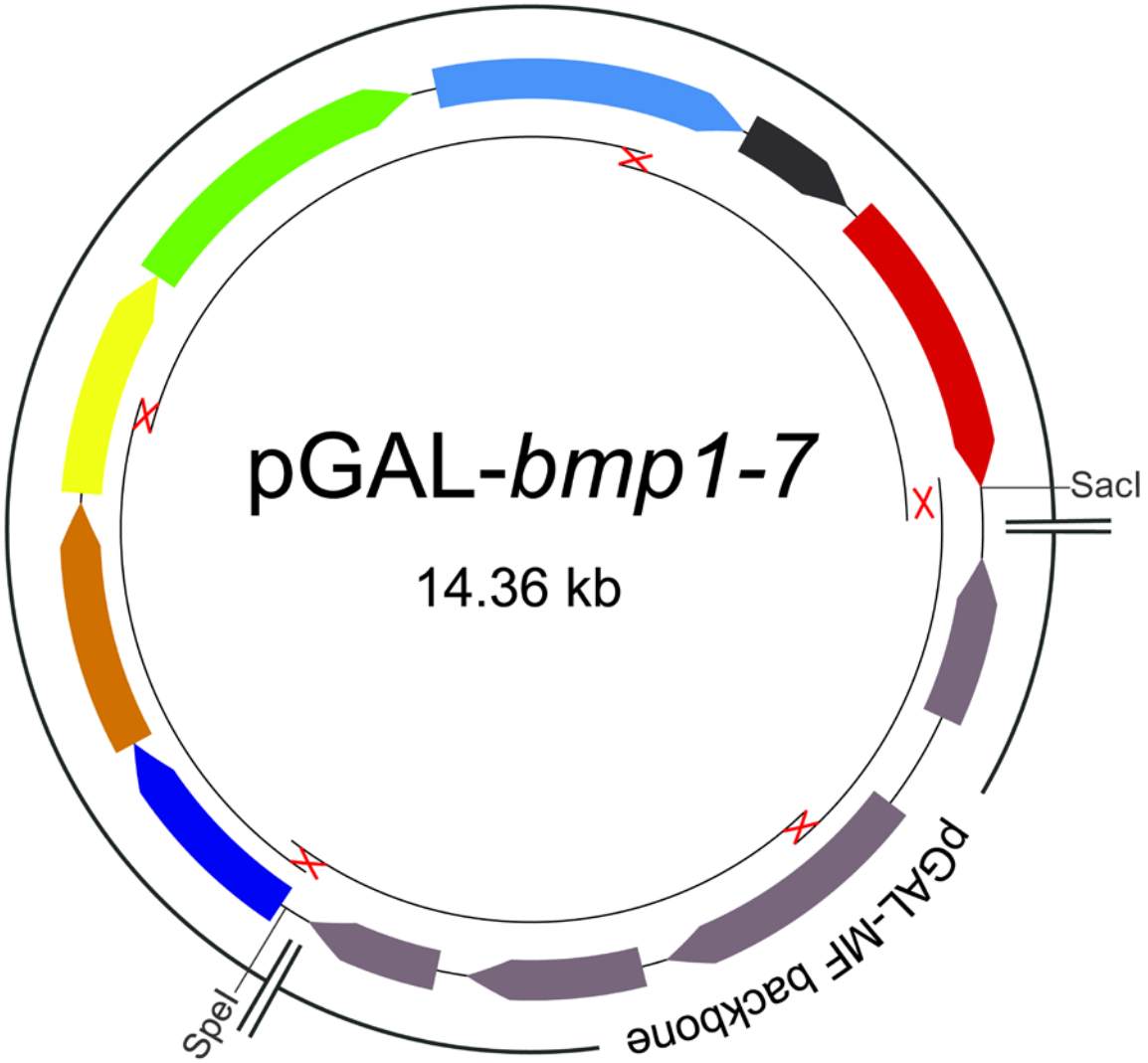

Supplementary Fig. 4. pGAL-*bmp1*–7 yeast/*E. coli* shuttle vector. pGAL-*bmp1–7* yeast/*E. coli* shuttle vector was assembled in *S. cerevisiae* BJ5465 from PCR amplified fragments (for primers see **Supplementary Table 3**).

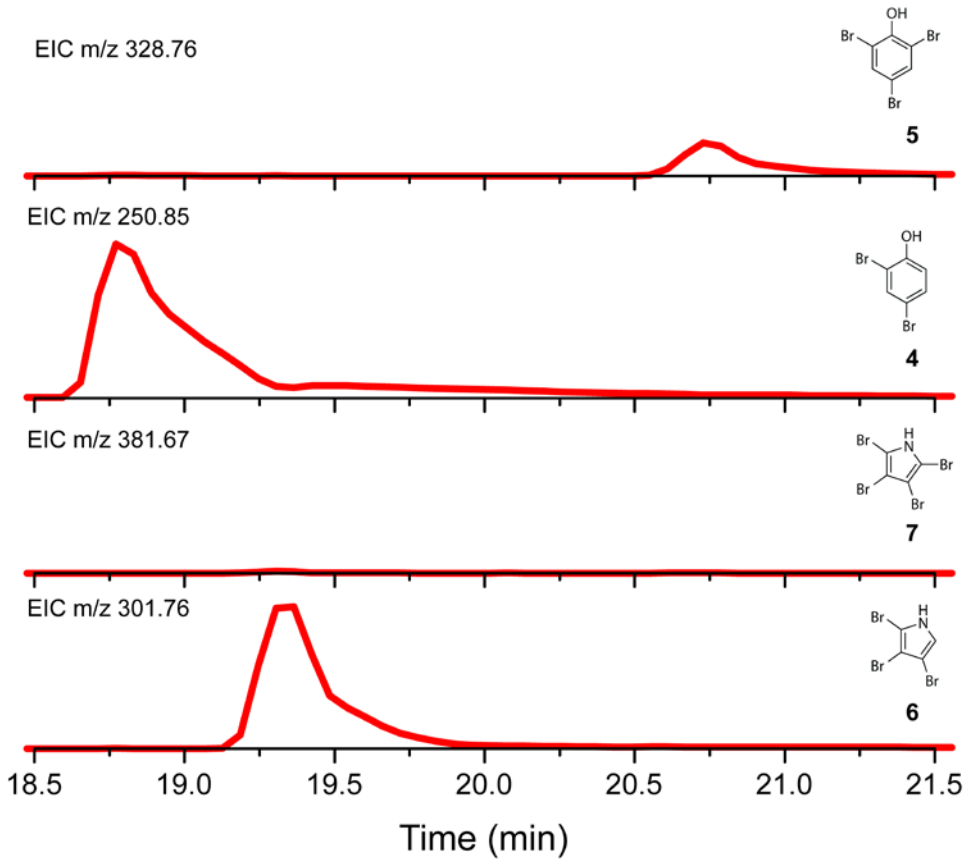

Supplementary Fig. 5. Chemotype for *bmp7* deletion. Deletion of *bmp7* from the heterologous expression vector pETDuet-*bmp1–7* results in accumulation of pyrrole and phenol monomers **4**–**6** in *E. coli*. Notably absent is **7**, which likely arises as a byproduct of dehalogenative radical coupling catalyzed by Bmp7. The figure shows EICs for the most abundant ions corresponding to each compound (the y-axis scale is identical for all plots).

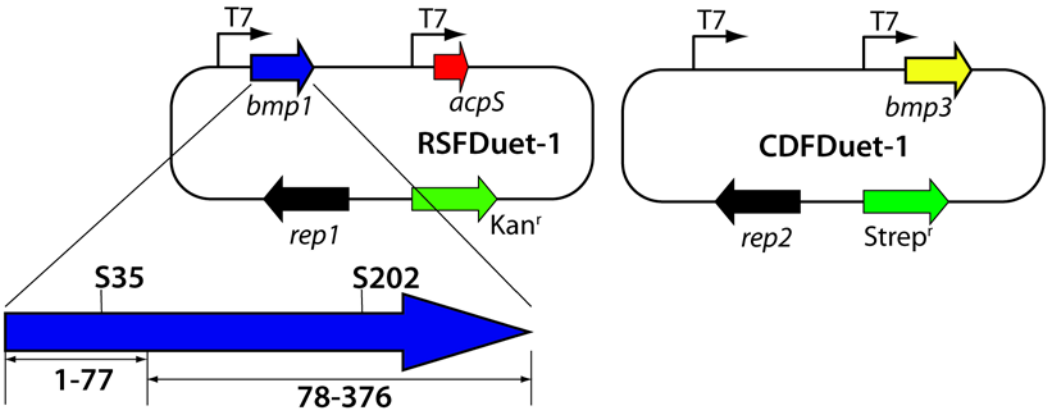

Supplementary Fig. 6. Plasmids for co-expression of *bmp1* with *bmp3*. Upon coexpression of the above two plasmids in *E. coli* BL21Gold(DE3), Bmp1(ACP) could be purified in complex with Bmp3. Purified Bmp1(ACP)-Bmp3 complex was subsequently used for assays with Bmp4 as described in **Supplementary Fig. 8**.

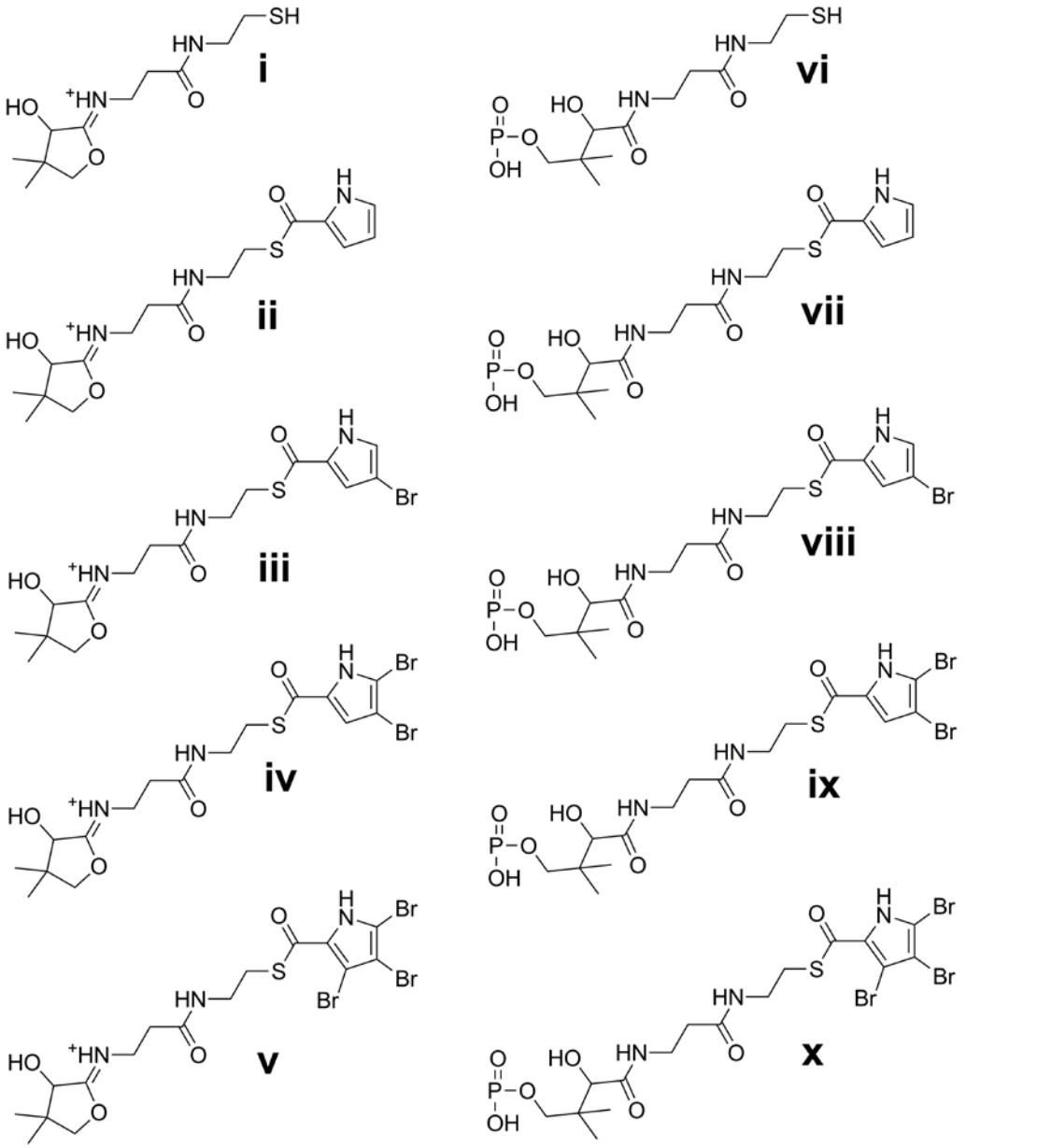

Supplementary Fig. 7. MS2 product ions corresponding to phosphopantetheine, phosphopantetheine acylated with pyrrole, and subsequent brominated states of the pyrrole. Note that the sites for the mono- and di-bromination for the pyrrole have been assumed as characterized for the pyrrole chlorinase PltA (**Supplementary Fig. 3**). The masses for the MS2 ions are listed. Under the experimental conditions in this study, MS2 product ions **i–v** were observed.

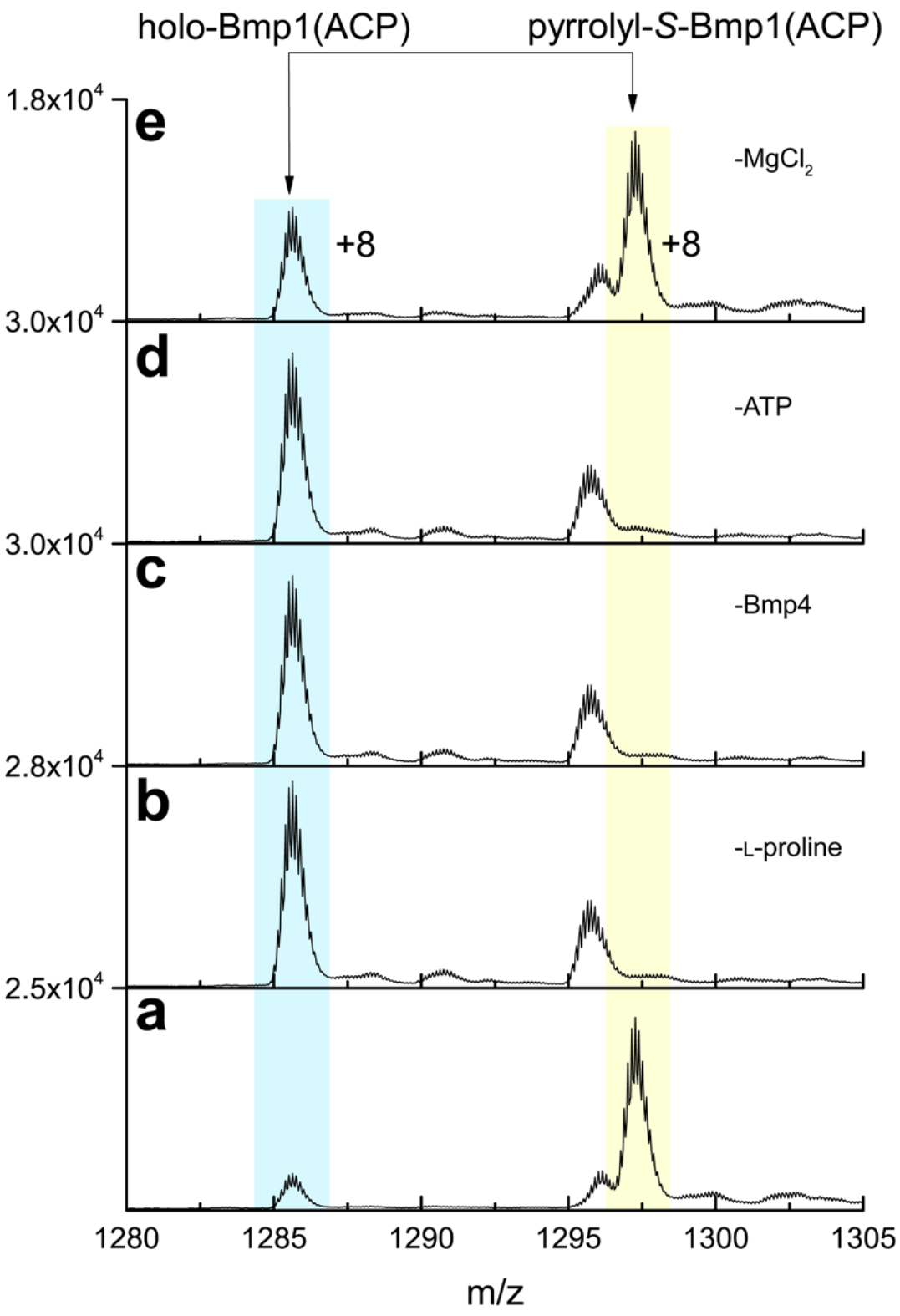

Supplementary Fig. 8. Enzymatic synthesis of pyrrolyl-*S*-Bmp1(ACP) by Bmp3 and Bmp4. (**a**) 40 µM of Bmp1(ACP)-Bmp3 complex, purified as described in **Supplementary Fig. 6** was incubated with 1 µM purified Bmp4, 4 mM L-proline, 2 mM ATP, 2 mM DTT and 10 mM $MgCl_2$ for 3 h at 30 °C in 100 mM potassium phosphate (pH 7.6) buffer.

Reaction components (**b**) ATP, (**c**) Bmp4, (**d**) L-proline, and (**e**) $MgCl_2$ were individually deleted and replaced with buffer. The assays were analyzed by LC-MS/MS. A peptide fragment corresponding to holo-Bmp1(ACP) (shaded blue) was identified by a diagnostic MS2 ion corresponding to species **i** as shown in **Supplementary Fig. 7**, while a peptide fragment corresponding to pyrrolyl-*S*-Bmp1(ACP) (shaded yellow) was identified by the diagnostic MS2 ion corresponding to species **ii** as shown in **Supplementary Fig. 7**. Both peptides were found to bear +8 charges as determined by their MS1 isotopic mass distribution. For illustrative purposes, MS1 spectra were summed over an identical 4 min time window during which both holo-Bmp1(ACP) and pyrrolyl-*S*-Bmp1(ACP) peptides were found to elute.

In the presence of all reaction components, Bmp4 and Bmp3 catalyzed the conversion of holo-Bmp1(ACP) to pyrrolyl-*S*-Bmp1(ACP) (panel **a**). Elimination of ATP, Bmp4 or L-proline abolished the formation of pyrrolyl-*S*-Bmp1(ACP). However, elimination of $MgCl_2$ (panel **e**) only led to a partial reduction in activity of Bmp4. These findings are consistent with the well-accepted reaction mechanism of adenyltransferase enzymes, such as Bmp4, in which the amino acid (L-proline for Bmp4) is activated by adenylation (derived from ATP), and subsequently transferred on to the terminal sulfhydryl of the phosphopantetheine arm of the holo-ACP.

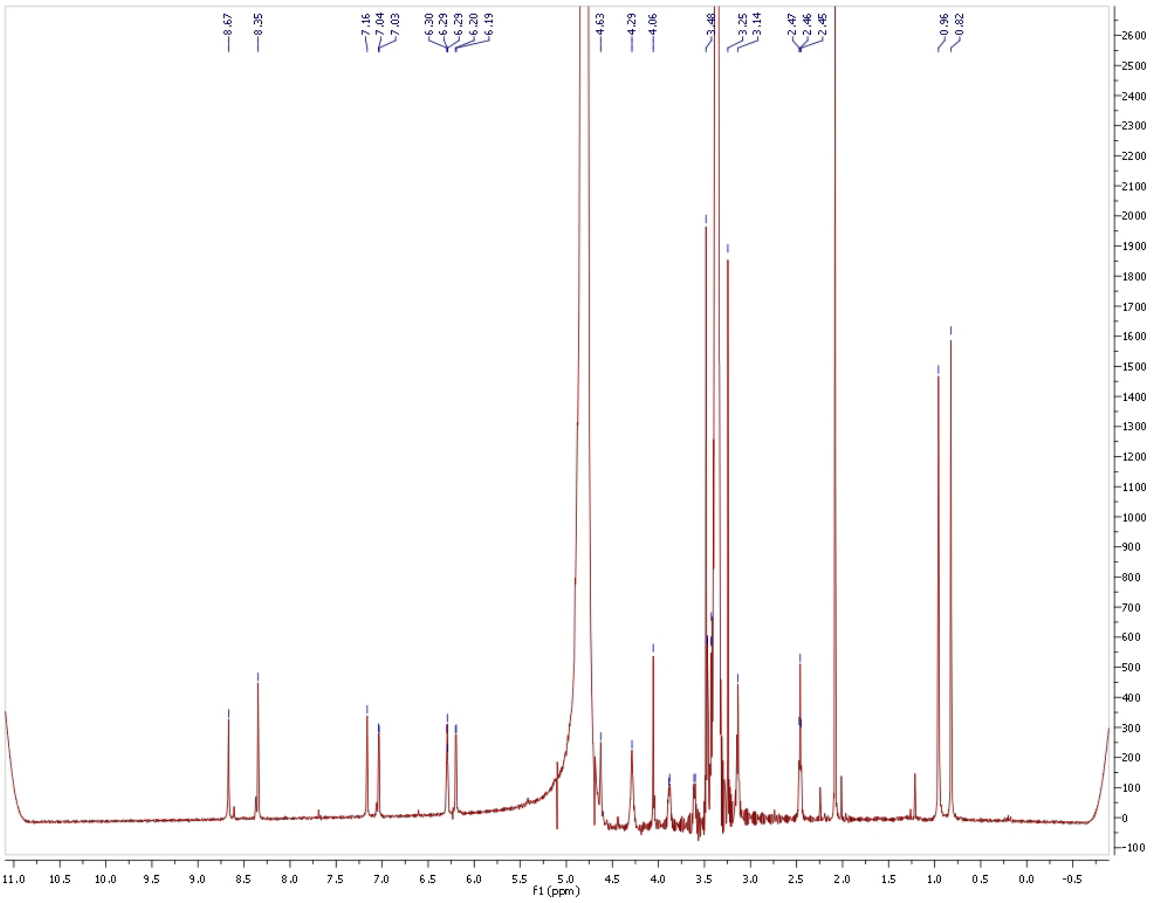

Supplementary Fig. 9. ^{1}H NMR spectrum for 16.

^{1}H NMR (600 MHz, D_2O) δ 8.67 – 8.63 (m, 1H), 8.33 (s, 1H), 7.16 – 7.12 (m, 1H), 7.15 (d, *J* = 7 Hz, 1H), 6.29 – 6.26 (m, 1H), 6.18 (d, *J* = 10 Hz 1H), 4.63-4.62 (m, 1H), 4.30 – 4.23 (m, 2H), 4.04 (s, 1H), 3.88 – 3.84 (m, 2H), 3.61 – 3.57 (m, 2H), 3.48 – 3.46 (m, 1H), 3.45-3.43 (m 1H) 3.41 (m, 1H), 3.23 (s, 1H), 3.12 (m, 1H), 2.44 (t, *J* = 10 Hz, 2H), 0.94 (s, 3H), 0.80 (s, 3H).

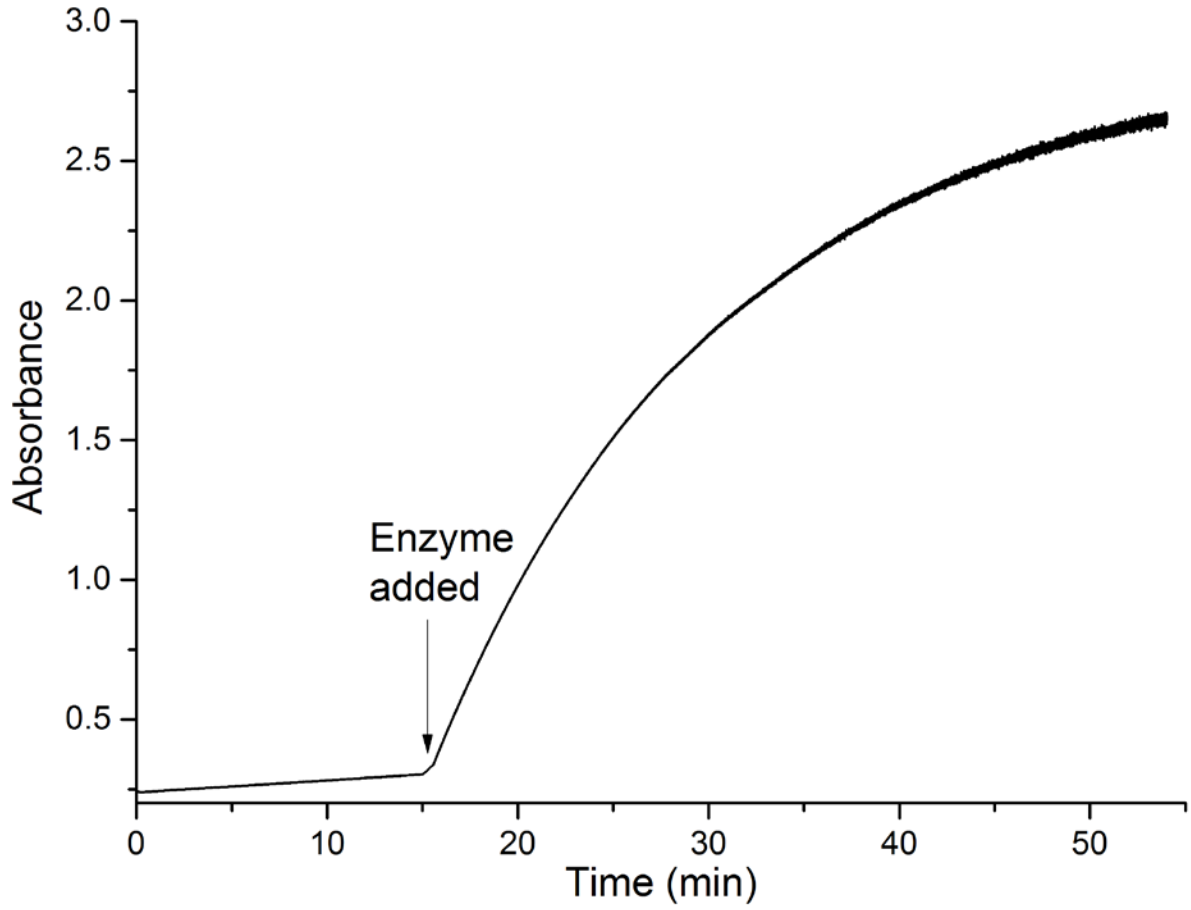

Supplementary Fig. 10. Hydrolysis of model esterase substrate p-nitrophenyl acetate (pNPA) by Bmp1(TE). 5 µM of purified Bmp1(TE) was used as the catalyst for the hydrolysis of 250 µM freshly prepared pNPA in 100 mM potassium phosphate (pH 7.6) buffer at room temperature. The reaction was monitored spectrophotometrically at wavelength of 400 nm in a quartz cuvette. Observed absorbance is plotted against time. Upon addition of enzyme, we observed significant increase in the hydrolysis of pNPA (denoted by the absorbance increase due to production of p-nitrophenol), implying that Bmp1(TE) catalyzed the hydrolysis of pNPA.

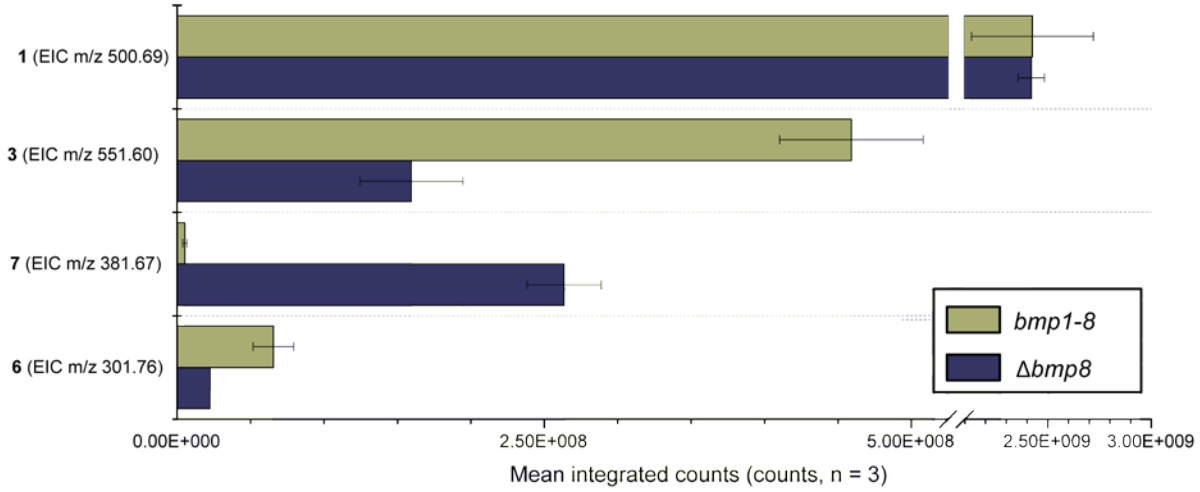

Supplementary Fig. 11. Chemotype for heterologous expression of *bmp1–7* omitting *bmp8*. Expression in *E. coli* of *bmp1-7* omitting *bmp8* results in decreased levels of **3** and **6** with a concomitant increase in **7**; **1** is shown as a control. Cultures of *E. coli* expressing the full *bmp* cluster or full *bmp* cluster excluding *bmp8* were grown in triplicate, extracted, and analyzed by LC-MS/MS as previously described. Levels of **3**, **6**, and **7** were quantified by peak integration of extracted ion chromatograms (EICs) corresponding to the most abundant ion for each compound. Means were calculated from each of three replicates for integrals taken from EICs for each ion and plotted, with the error bars representing standard deviations.

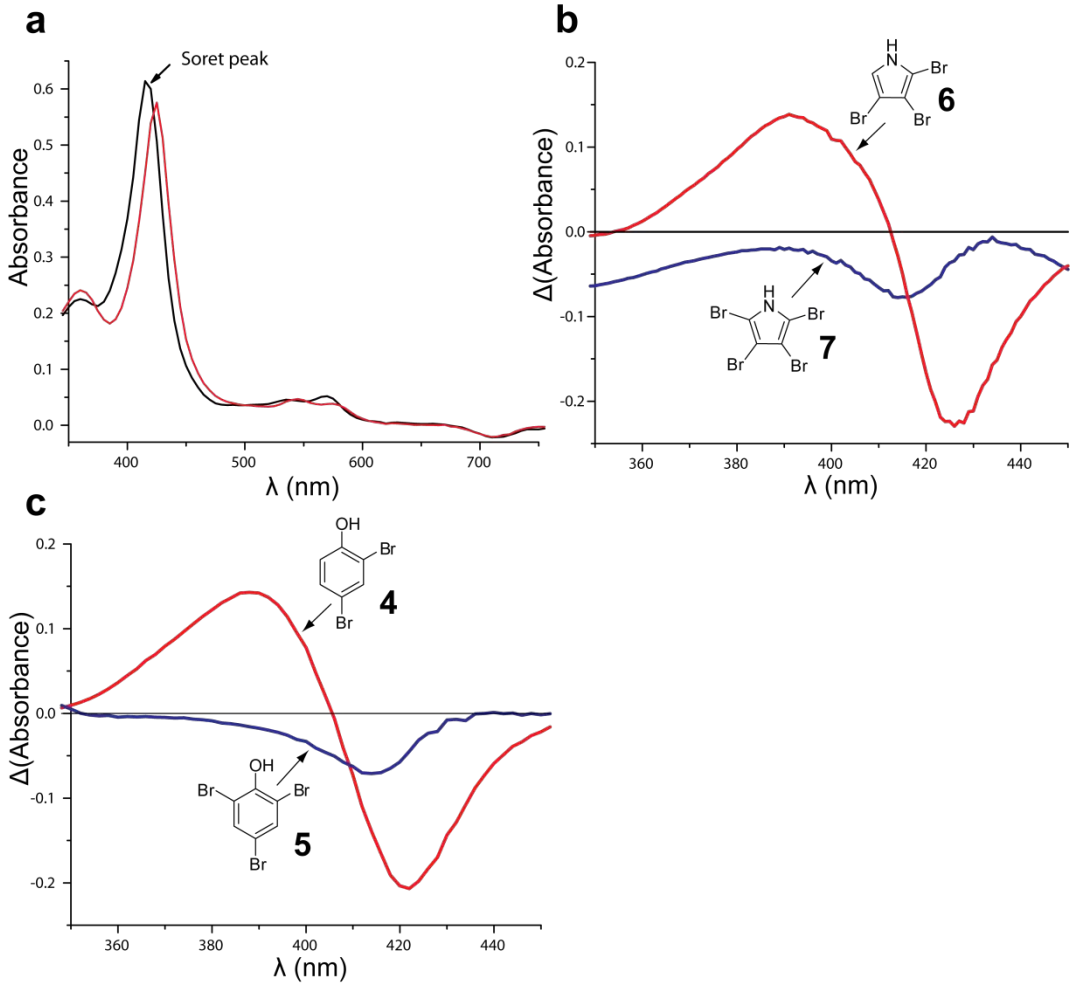

Supplementary Fig. 12. Spectral characteristics of CYP450 Bmp7 and spectrophotometric determination of substrate tolerance. (**a**) An absorbance scan for 5 µM purified Bmp7 in 100 mM potassium phosphate buffer (pH 7.6) was performed using a Cary-40 UV-Vis spectrophotometer in a quartz cuvette. Bmp7 demonstrates a typical CYP450 absorbance curve, with a Soret peak at 415 nm (black curve) upon addition of 1mM imidazole (red curve). (**b**) **6** was synthesized according to published protocols[10]. Difference absorbance spectra upon titration of Bmp7 with 200 µM **6** or **7** identify binding of **6** in a manner characteristic for substrates of CYP450 enzymes; note that **7** does not yield a similar absorbance change. (**c**) Similarly, a difference absorbance spectra upon titration of Bmp7 with **4** or **5** identifies binding of **4** characteristic for substrates of CYP450 enzymes.

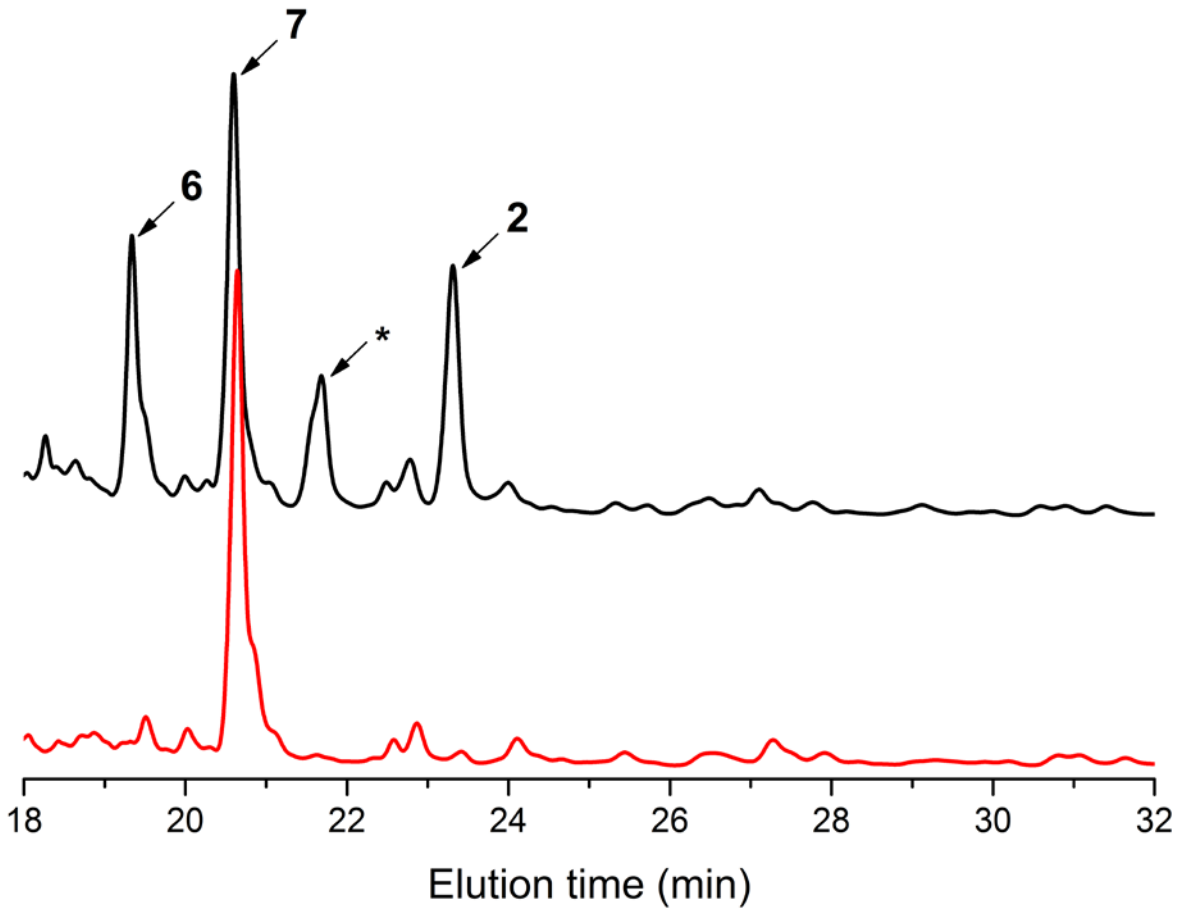

Supplementary Fig. 13. ***In vitro*** **Bmp7 reaction products with 6 (black, top curve) and 7 (bottom, red curve) as substrates.** With **6** as a substrate, Bmp7 generated three distinct products, **2**, **7**, and an uncharacterized species corresponding to pentabromo-bipyrrole (marked by *, having a molecular formula $C_8H_3Br_5N_2$ as predicted from MS1 spectrum). This product could not be generated in quantities sufficient for complete structure elucidation. The pentabromo-bipyrrole product can be rationalized on the basis of dehalogenated-aryl coupling polybrominated biphenyl and OH-BDE products **10**, **12** and **14** (*vide infra*). Upon reaction with **7**, no product peaks could be observed.

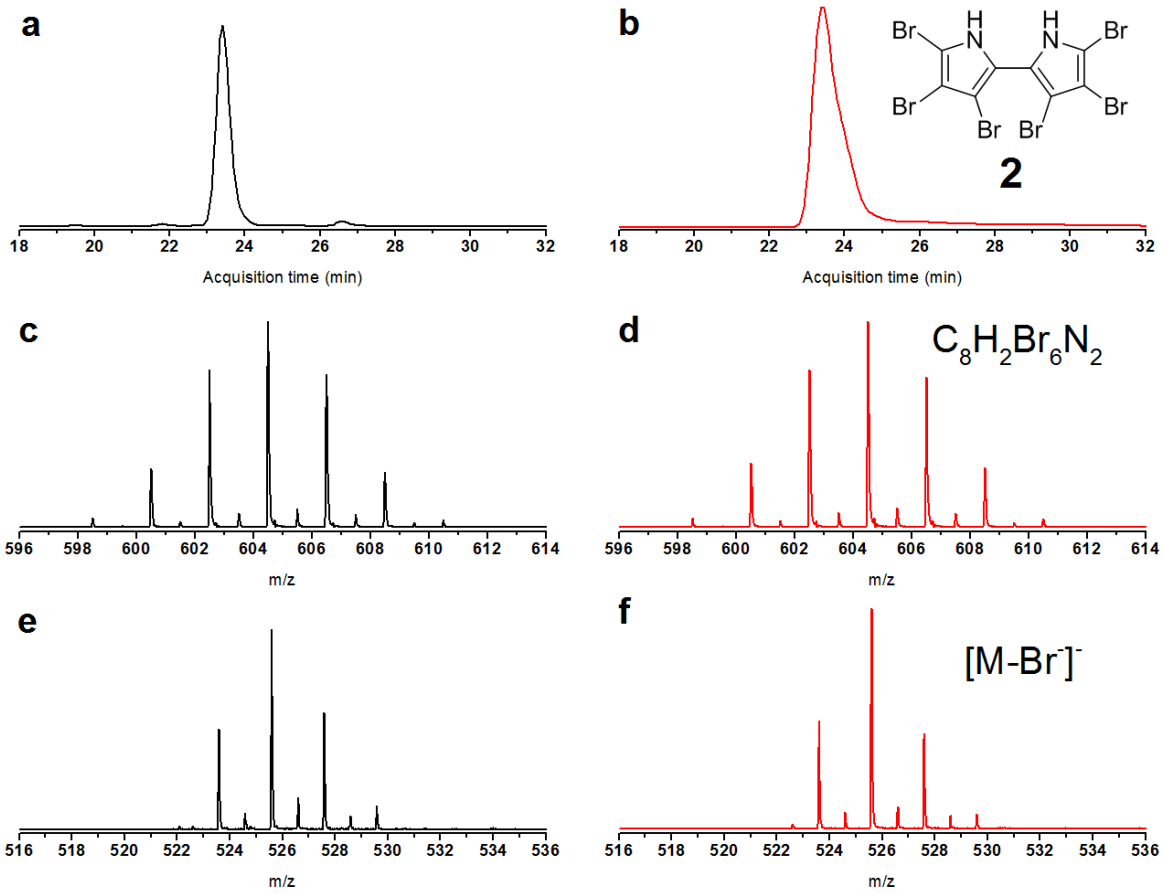

Supplementary Fig. 14. Characterization of 2 generated by Bmp7 *in vitro* reaction with 6 as a substrate. Extract of Bmp7 reaction (black curves) was compared to an authentic NMR characterized sample of **2** (red curves) isolated from *P. luteoviolacea* 2ta16. (**a**, **b**) Comparison of retention times. MS1 EIC corresponding to the most abundant isotope for the molecular formula $C_8H_2Br_6N_2$ (m/z =604.51, 10 ppm tolerance) for the Bmp7 reaction extract (**a**) and authentic standard of **2** (**b**) analyzed under identical chromatographic conditions. (**c**, **d**) Comparison of MS1 profiles. MS1 mass spectrum for species at retention time 23.4 min from the Bmp7 reaction extract (**c**) and authentic standard of **2** (**d**). (**e**, **f**) Comparison of MS/MS profiles. MS2 profile of the product ions generated from most abundant isotope MS1 ions corresponding to the molecular formula $C_8H_2Br_6N_2$ at identical retention times from the Bmp7 reaction extract (**e**) and authentic standard of **2** (**f**). Most abundant MS2 ions corresponded to the $[M-Br^-]^-$. Identical retention times, MS1 and MS/MS profiles as compared to a NMR characterized authentic standard lead to the characterization of the Bmp7 reaction product as **2**.

NMR spectra for **2** purified from preparative scale cultures of *P. luteoviolacea* 2ta16 and used as authentic standard in panels **b**, **d** and **f** above:

2: ^{1}H NMR: ($CDCl_3$) δ [ppm] 9.87 (bs, 1H); ^{13}C NMR: ($CDCl_3$) δ [ppm] 121.60, 115.37, 102.76, 100.98

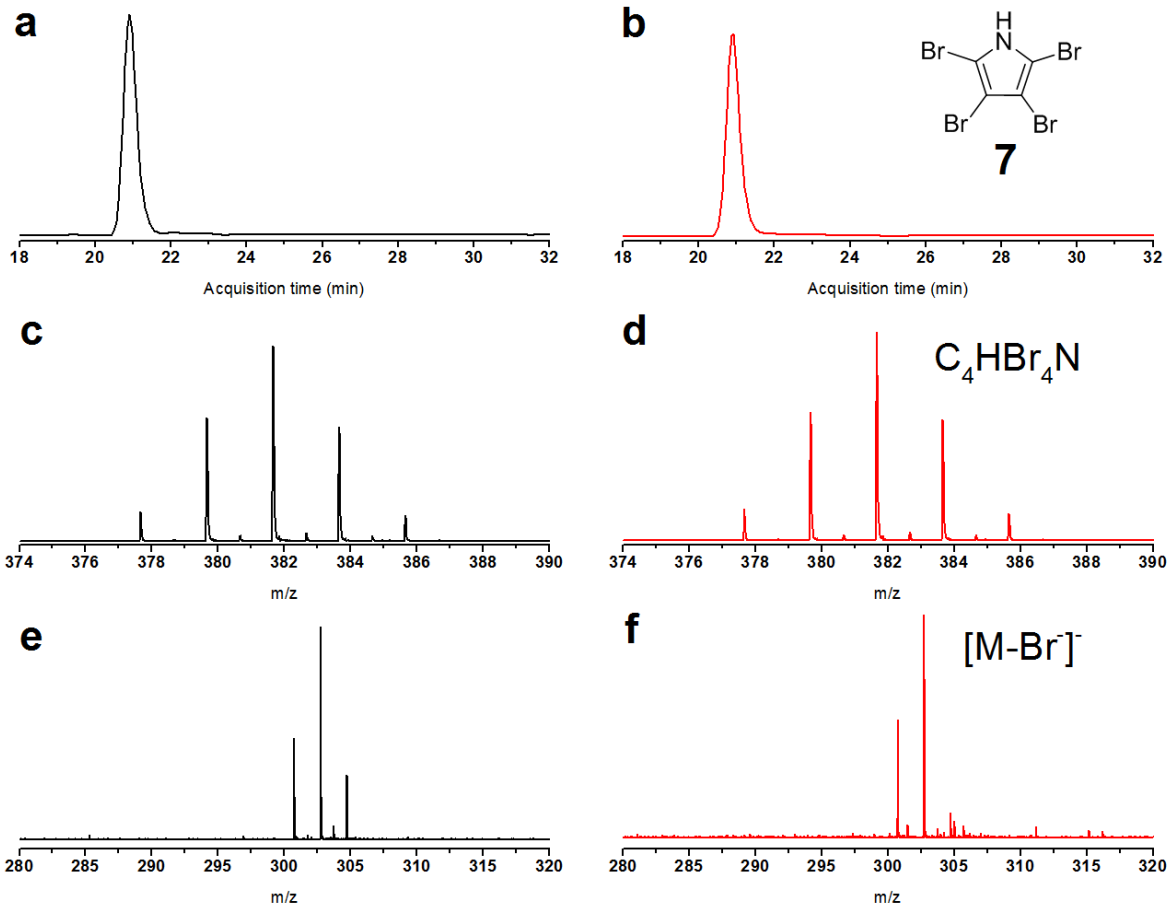

Supplementary Fig. 15. Characterization of 7 generated by Bmp7 *in vitro* reaction with 6 as a substrate. Extract of Bmp7 reaction (black curves) was compared to an authentic commercial synthetic standard of **7** (Sigma-Aldrich, L165042-50MG) (red curves). (**a**, **b**) Comparison of retention times. MS1 EIC corresponding to the most abundant isotope for the molecular formula C_4HBr_4N (m/z = 381.67, 10 ppm tolerance) for the Bmp7 reaction extract (**a**) and authentic standard of **7** (**b**) analyzed under identical chromatographic conditions. (**c**, **d**) Comparison of MS1 profiles. MS1 mass spectrum for species at retention time 20.8 min from the Bmp7 reaction extract (**c**) and authentic standard of **7** (**d**). (**e**, **f**) Comparison of MS/MS profiles. MS2 profile of the product ions generated from most abundant isotope MS1 ions corresponding to the molecular formula C_4HBr_4N at identical retention times from the Bmp7 reaction extract (**e**) and authentic standard of **7** (**f**). Most abundant MS2 ions corresponded to the $[M\text{-}Br^-]^-$. Identical retention times, MS1 and MS/MS profiles as compared to an authentic synthetic standard lead to the characterization of the Bmp7 reaction product as **7**.

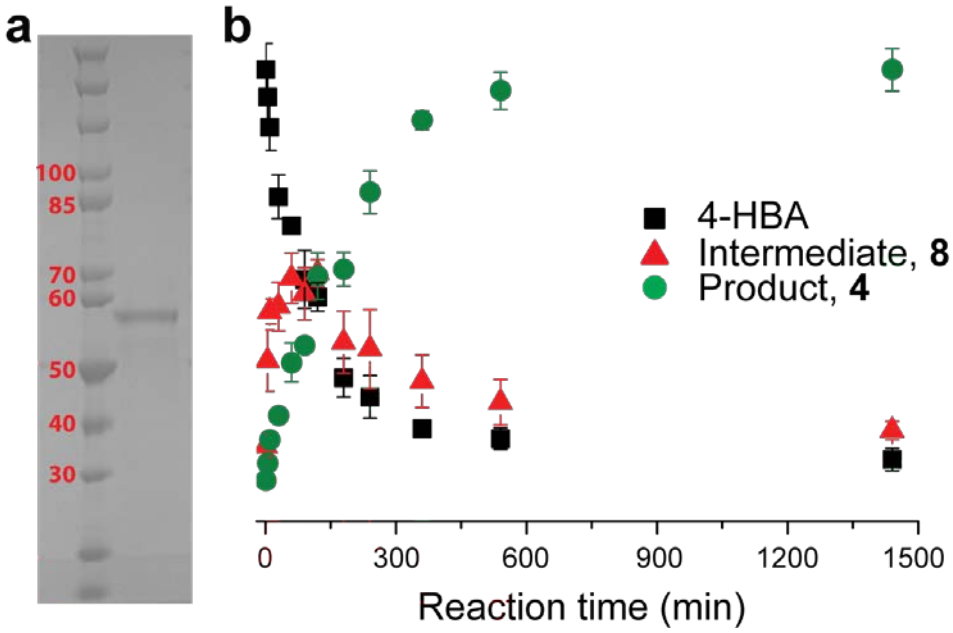

Supplementary Fig. 16. Purification of recombinant Bmp5 and time course for the change in concentrations of the substrate, intermediate and product species as shown in Fig. 4a. (**a**) Affinity chromatography purified Bmp5 is analyzed by SDS-PAGE, along with molecular weight marker (Fisher Scientific BP3602) with molecular weights listed in red in kDa. The expected molecular weight for N-His_6-Bmp5 is 61 kDa (**b**) Area under the substrate, intermediate and product peaks as shown in **Fig. 4a** were integrated, and mean values from three independent experiments were plotted against reaction time with error bars representing standard deviation. The intermediate and product were identified to be **8** and **4** respectively by high-resolution mass spectrometry and comparison of retention times to authentic synthetic standards.

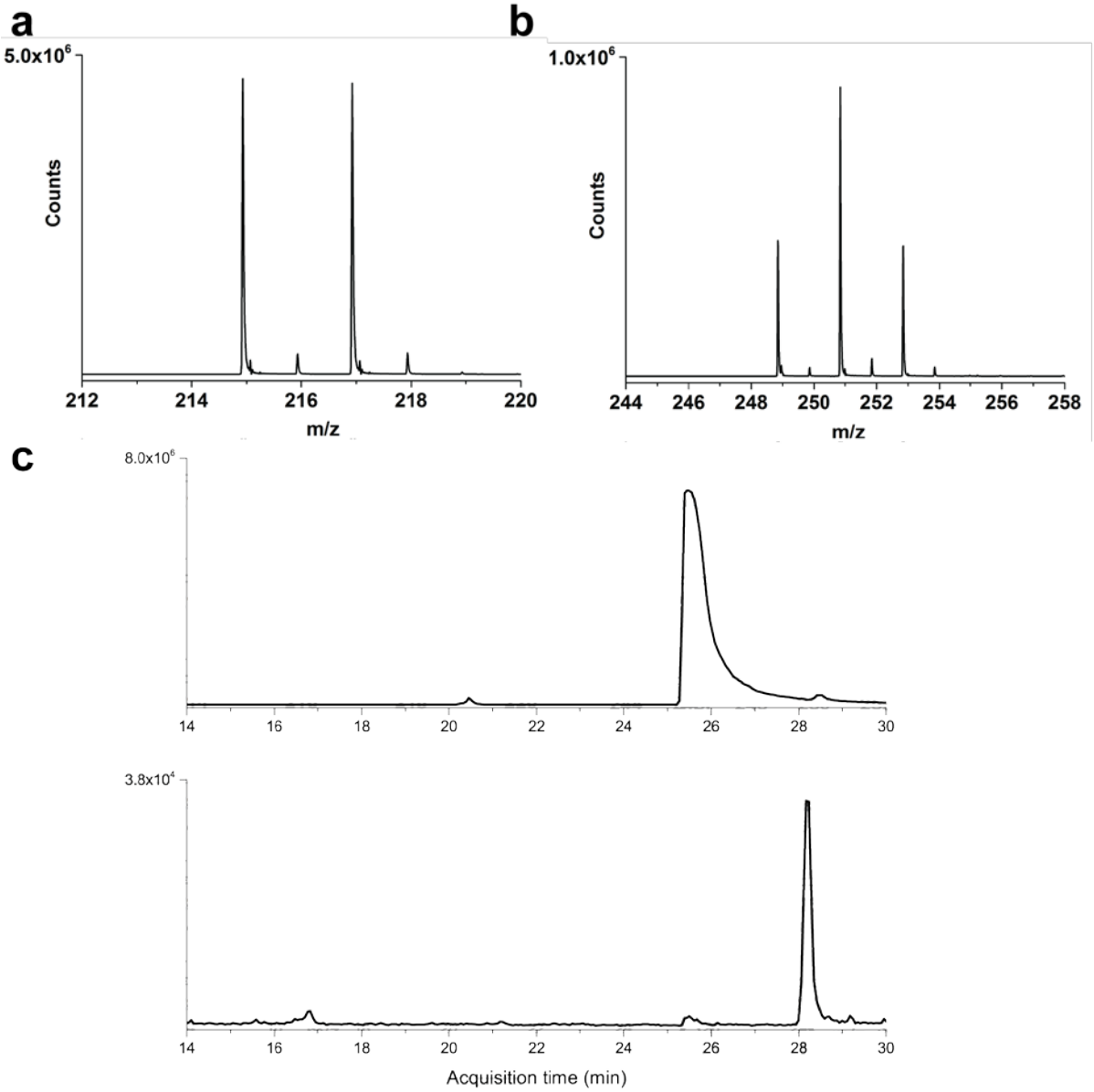

Supplementary Fig. 17: Mass spectra for 8 and 4, and *in vivo* production of 4 and 5 by Bmp5. The mass spectra for (**a**) Bmp5 intermediate **8** and (**b**) Bmp5 product **4** generated by *in vitro* reaction of Bmp5 with 4-HBA led to the assignment of the chemical formulae as $C_7H_5O_3Br$ and $C_6H_4OBr_2$ respectively. (**c**) MS1 EIC for m/z = 248.85 (10 ppm tolerance) and m/z = 326.766 (10 ppm tolerance) showing the production of **4** (top) and **5** (bottom) when Bmp5 was expressed in *E. coli* in LB media supplemented with 1 g/L KBr. Assuming identical ionization for **4** and **5**, it can be discerned that **4** is the major product generated by Bmp5.

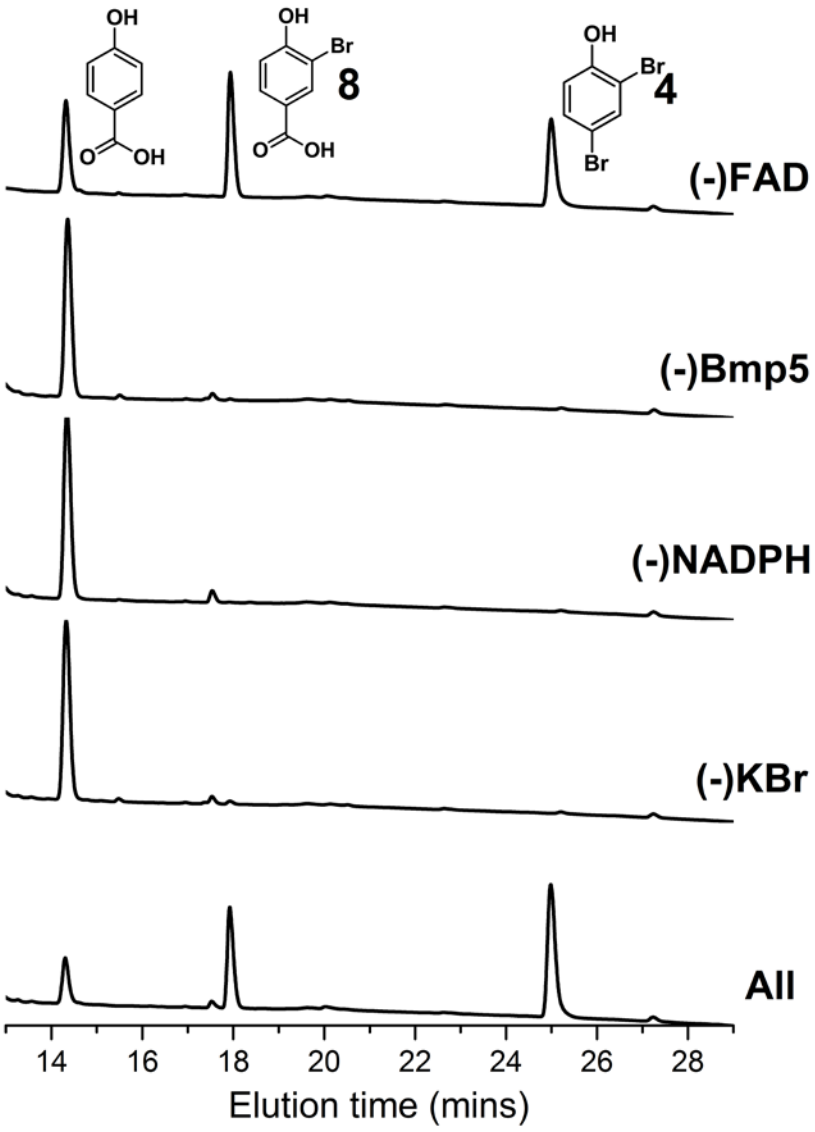

Supplementary Fig. 18. Negative control reactions demonstrate the requirement of KBr and NADPH for catalysis by Bmp5. No conversion of 4-HBA to **8** and **4** was observed when Bmp5, NADPH or KBr were omitted from the Bmp5 *in vitro* assay. Omission of FAD did not abolish enzyme activity, but lowered substrate turnover.

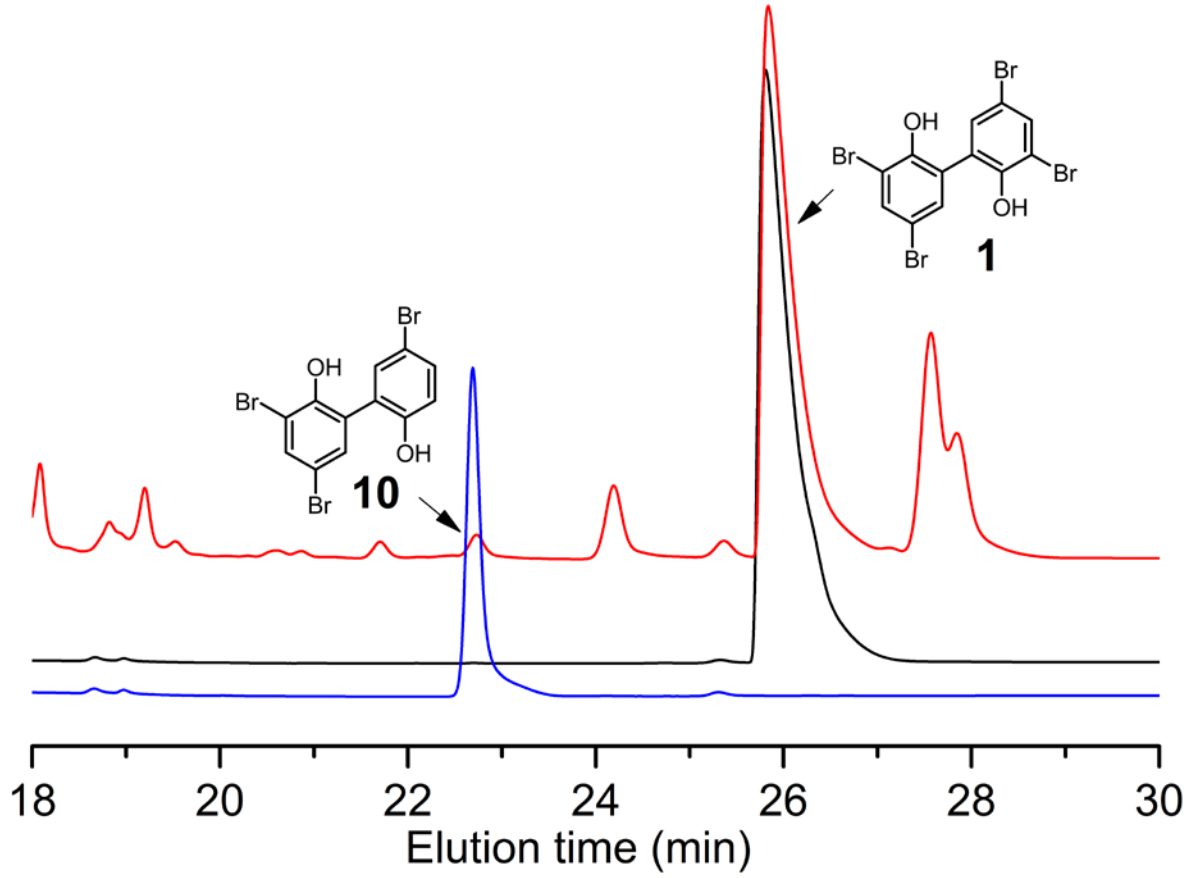

Supplementary Fig. 19. Comparison of retention times and NMR spectra of polybrominated biphenyl products 1 and 10 generated by Bmp7 *in vitro* with authentic synthetic standards. Extract of Bmp7 reaction with **4** (red curve) was analyzed using identical chromatographic conditions as for authentic synthetic standards of **1** (black curve) and **10** (blue curve). Note that retention times for authentic standards of **1** and **10** match those for two separate product peaks from the enzymatic reaction leading to the identification of the chemical structures of these species. Synthetic standard of **1** was obtained from Sigma-Aldrich (S842753-50MG) and dissolved in 1 mL DMSO. Analysis by LC-MS/MS identified two major peaks in roughly 80:20 relative abundance with respective molecular formulae as $C_{12}H_6O_2Br_4$ and $C_{12}H_7O_2Br_3$. Both products were purified by semi-preparative scale HPLC. After drying *in vacuo*, 500 µg of each product was dissolved in 50 µL DMSO, and ^{1}H NMR spectra were acquired. By molecular formulae, MS/MS fragmentation patterns, and comparison of NMR spectra to literature[3-4], the identity of the synthetic standard of **1** and for the synthetic standard of **10** can be discerned as shown above. This lead to the identification of **1** and **10** as products generated by Bmp7.

The ^{1}H NMR chemical shifts of the synthetic standards of **1** and **10**, which are in good agreement to literature values, are as follows:

1: ^{1}H NMR (600 MHz, $CDCl_3$) δ 7.65 (d, *J* = 2.3 Hz, 1H), 7.31 (d, *J* = 2.3 Hz, 1H).

10: ^{1}H NMR (600 MHz, $CDCl_3$) δ 7.67 (d, *J* = 2.3 Hz, 1H), 7.39 (dd, *J* = 8.6, 2.4 Hz, 1H), 7.37 (d, *J* = 2.3 Hz, 1H), 7.34 (d, *J* = 2.4 Hz, 1H), 6.90 (d, *J* = 8.6 Hz, 1H).

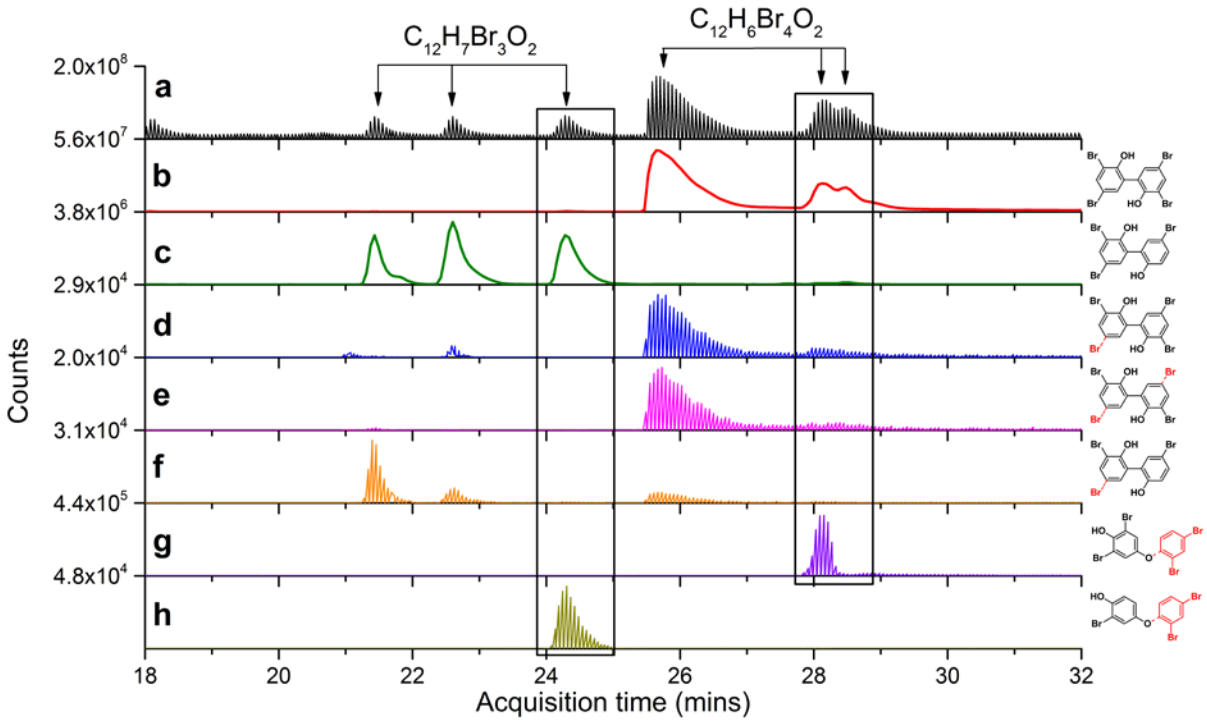

Supplementary Fig. 20. Mass spectrometric analysis of the polybrominated biphenyls, and OH-BDE products generated by Bmp7. (**a**) Total ion chromatogram (TIC) for the Bmp7 reaction extract. Peaks corresponding to the three isomers each for the major products corresponding to the molecular formulae $C_{12}H_7Br_3O_2$ and $C_{12}H_6Br_4O_2$ are indicated. (**b**) MS1 extracted ion chromatogram (EIC) corresponding to the most abundant ion for molecular formula $C_{12}H_6Br_4O_2$ (m/z = 500.69, 10 ppm tolerance) identifies a set of three distinct isomeric product peaks. Chemical structure for **1** is shown on the right. (**c**) MS1 EIC corresponding to the most abundant ion for molecular formula $C_{12}H_7Br_3O_2$ (m/z = 420.79, 10 ppm tolerance) identifies a second set of three distinct isomeric product peaks. The chemical structure for **10** is shown on the right. (**d**) EIC corresponding to MS2 product ion $[M\text{-}Br^-]^-$ from $C_{12}H_6Br_4O_2$ (m/z = 421.78, 10 ppm tolerance). (**e**) EIC corresponding to MS2 product ion $[M\text{-}2Br^-]^-$ from $C_{12}H_6Br_4O_2$ (m/z = 339.85, 10 ppm tolerance). (**f**) EIC corresponding to MS2 product ion $[M\text{-}Br^-]^-$ from $C_{12}H_7Br_3O_2$ (m/z = 340.86, 10 ppm tolerance). (**g**) EIC corresponding to dibromobenzoquinone MS2 product ion generated from $C_{12}H_6Br_4O_2$ (m/z = 265.84, 10 ppm tolerance). Chemical structure for **11** with the loss of dibromobenzene (in red) is shown on the right. (**h**) EIC corresponding to bromobenzoquinone MS2 product ion generated from $C_{12}H_7Br_3O_2$ (m/z = 185.93, 10 ppm tolerance). Chemical structure for **12** with the loss of dibromobenzene (in red) is shown on the right. Note that para-OH-BDEs (**11–12**) possess a MS/MS signature typified the detection of a bromobenzoquinone MS fragment ion, while ortho-OH-BDEs (**13**) are not fragmented.

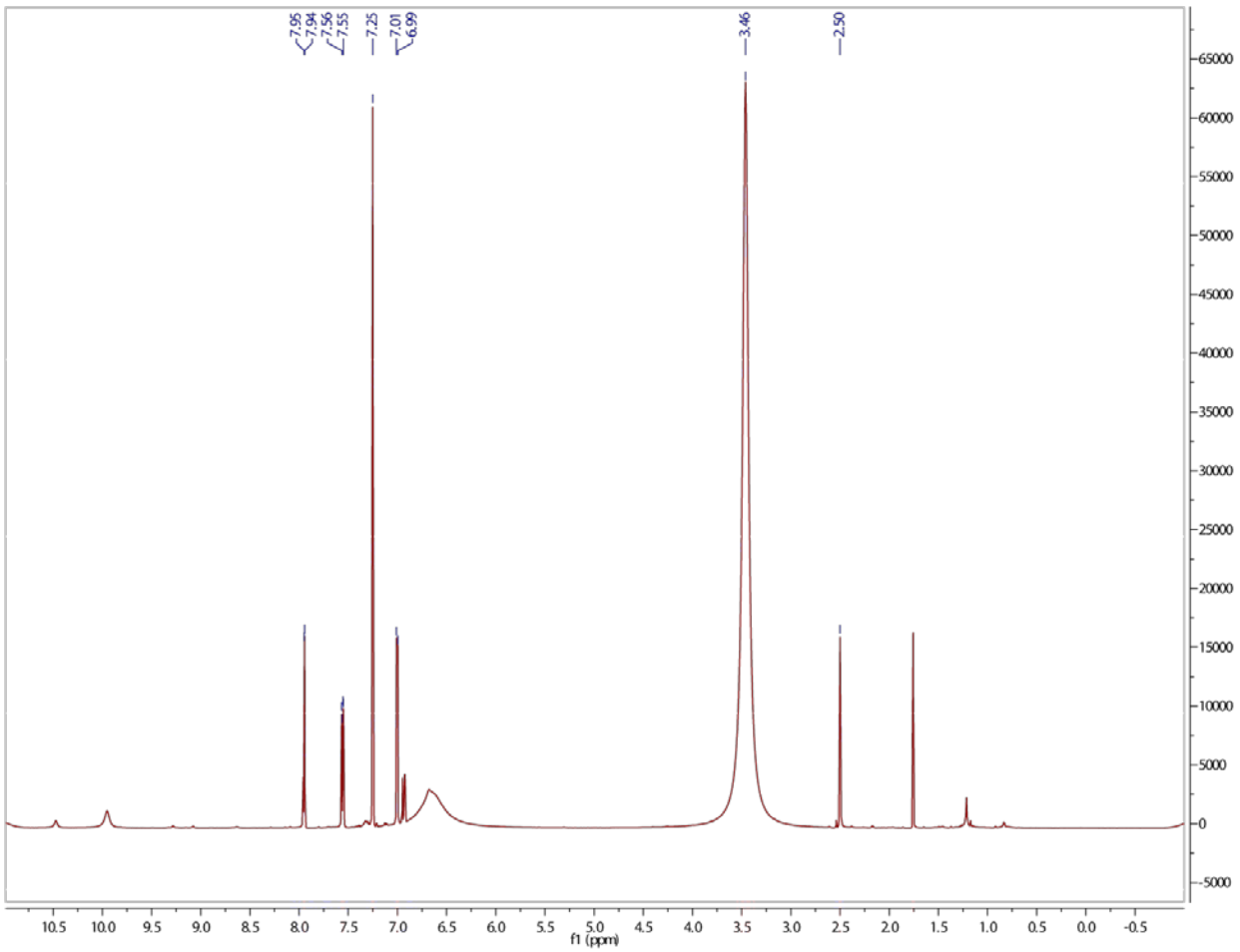

Supplementary Fig. 21. ^{1}H NMR spectrum for 11.

11: ^{1}H NMR (600 MHz, DMSO) δ 7.95 (d, *J* = 2.4 Hz, 1H), 7.56 (dd, *J* = 8.8, 2.3 Hz, 1H), 7.25 (s, 2H), 7.00 (d, *J* = 8.7 Hz, 1H).

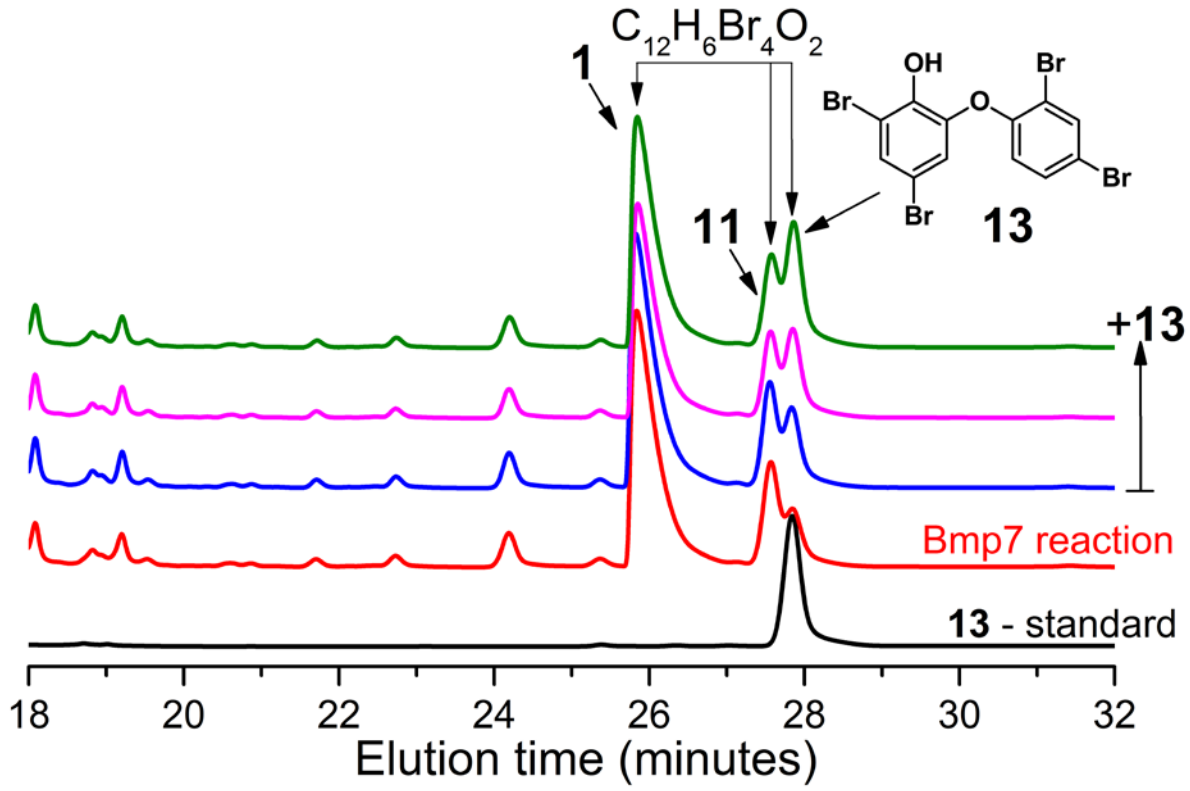

Supplementary Fig. 22. Identification of 2′-OH-BDE-68 (13) as a reaction product generated by Bmp7. Bmp7 produces three isomeric products of molecular formula $C_{12}H_6Br_4O_2$. Products **1** and **11** had been identified by comparison to authentic standard for **1** (**Supplementary Fig. 19**), and comprehensive structural characterization by NMR spectroscopy for **11** (**Supplementary Note 2** and **Supplementary Fig. 21**). Extract of *in vitro* reaction of Bmp7 with **4** (red trace) was supplemented with a synthetic standard of **13** in increments of 0.25 µg each. Note that of the three isomeric peaks with $C_{12}H_6Br_4O_2$ molecular formula, supplementation with authentic standard identifies the third peak with retention time ~ 27.8 min as **13**.

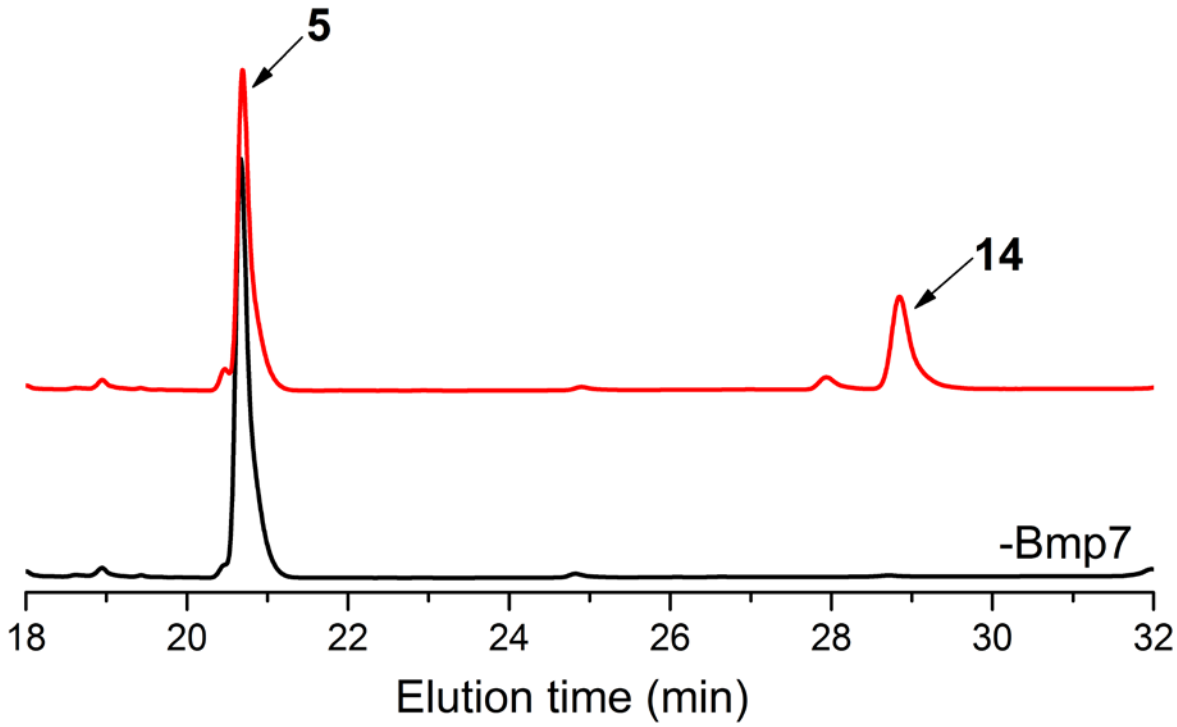

Supplementary Fig. 23. HPLC detection of products generated by Bmp7 using 5 as a substrate. Curve in black represents a negative control reaction in which Bmp7 was omitted. Only a single brominated product was identified (red curve). Note that the substrate (**5**) has only been partially consumed.

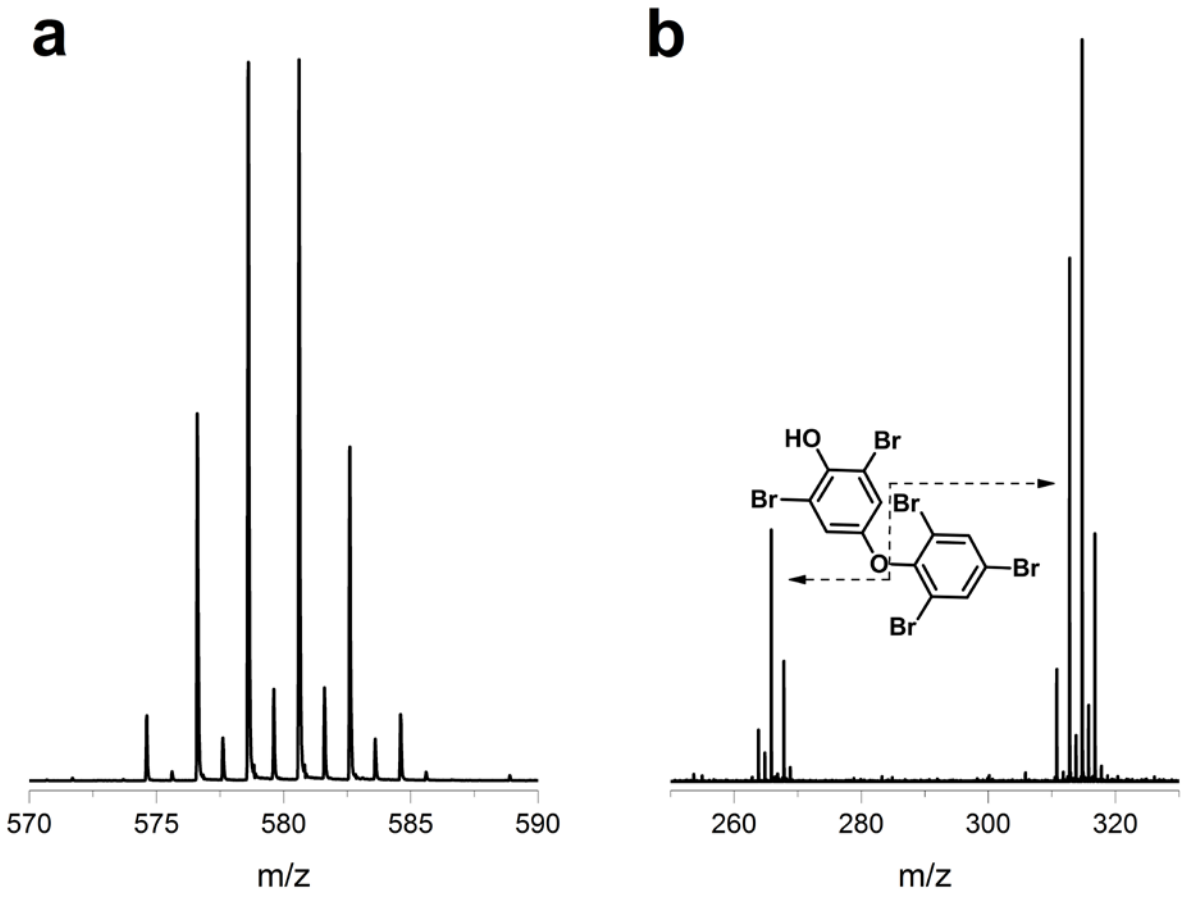

Supplementary Fig. 24. MS and MS/MS profiles for 14, produced enzymatically by reaction of Bmp7 with 5. (**a**) MS1 isotope distribution for **14**. The mass and isotope distribution correspondes to the molecular formula $C_{12}H_5Br_5O_2$. (**b**) MS2 ions corresponding to the scission of ether bond in the structure of **14**. Two distinct MS2 ions can be detected, corresponding to dibromobenzoquinone and tribromobenzene as shown. Detection of the dibromobenzoquinone MS2 ion is consistent with **14** being a para-OH-BDE[8], as discussed in the **Supplementary Note 2** and **Supplementary Fig. 20**. The final deduced structure of **14** is shown with the appropriate fragment ions.

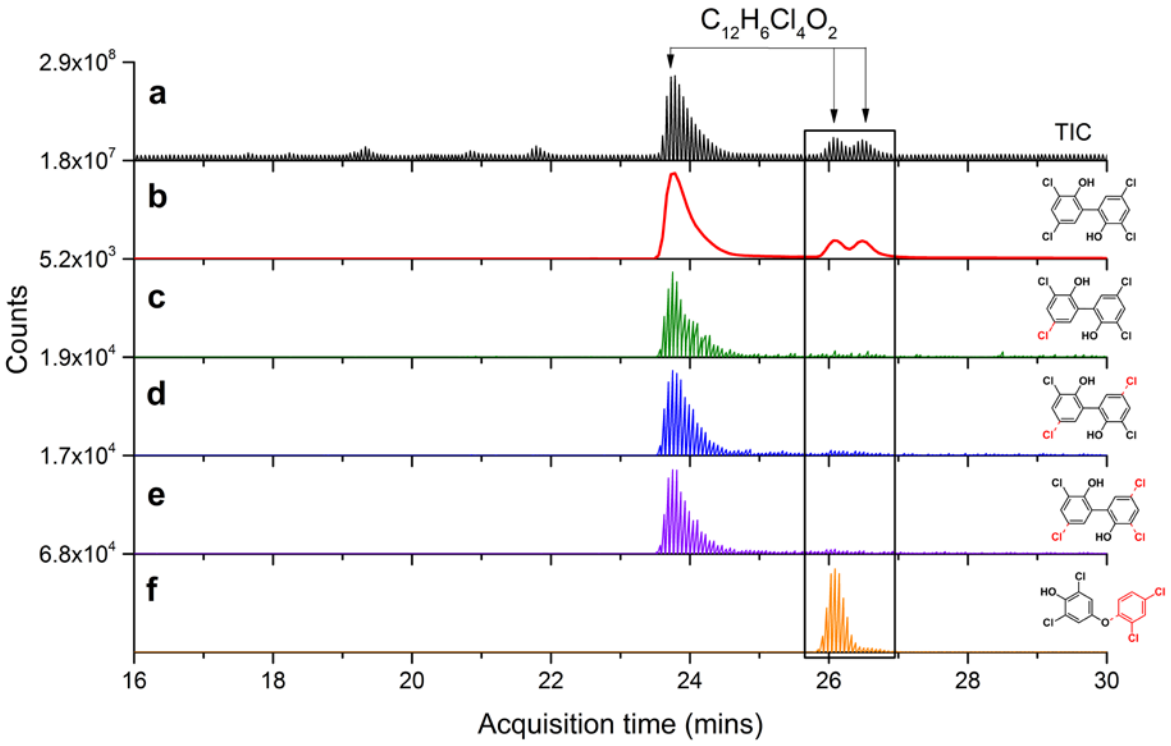

Supplementary Fig. 25. Mass spectrometric analysis of the biphenyl and hydroxylated diphenyl ether products formed by Bmp7 reaction with 17. (**a**) Total ion chromatogram (TIC) for the Bmp7 reaction extract. Peaks for the three isomeric major products corresponding to the molecular formulae $C_{12}H_6Cl_4O_2$ are indicated. (**b**) MS1 extracted ion chromatogram (EIC) corresponding to the most abundant ion for molecular formula $C_{12}H_6Cl_4O_2$ (m/z = 322.90, 10 ppm tolerance) identifies a set of three distinct isomeric product peaks. The postulated chemical structure for **18** is shown on the right. (**c**) MS2 EIC corresponding to $[M\text{-}Cl^-]^-$ (m/z = 286.92, 10 ppm tolerance). (**d**) MS2 EIC corresponding to $[M\text{-}2Cl^-]^-$ (m/z = 250.95, 10 ppm tolerance). (**e**) MS2 EIC corresponding to $[M\text{-}3Cl^-]^-$ (m/z = 222.95, 10 ppm tolerance). (**f**) MS2 EIC corresponding to dichlorobenzoquinone (m/z = 175.94, 10 ppm tolerance). The postulated chemical structure for **19** with the loss of dichlorobenzene (in red) is shown on the right. Note that of the three isomers, one isomers demonstrated the successive loss of chlorine atoms, leading to its postulated structure assignment as a polychlorinated biphenyl analogous to **1**. One of the isomers demonstrates a dichlorobenzoquinone MS2 product ion, leading to its postulated structure assignment as a para-hydroxyl diphenyl ether, analogous to **11**. The third isomer, with similar retention time to the para-hydroxy diphenyl ether, and not demonstrating any MS2 fragment ions is postulated to be an ortho-hydroxy diphenyl ether, analogous to **13**.

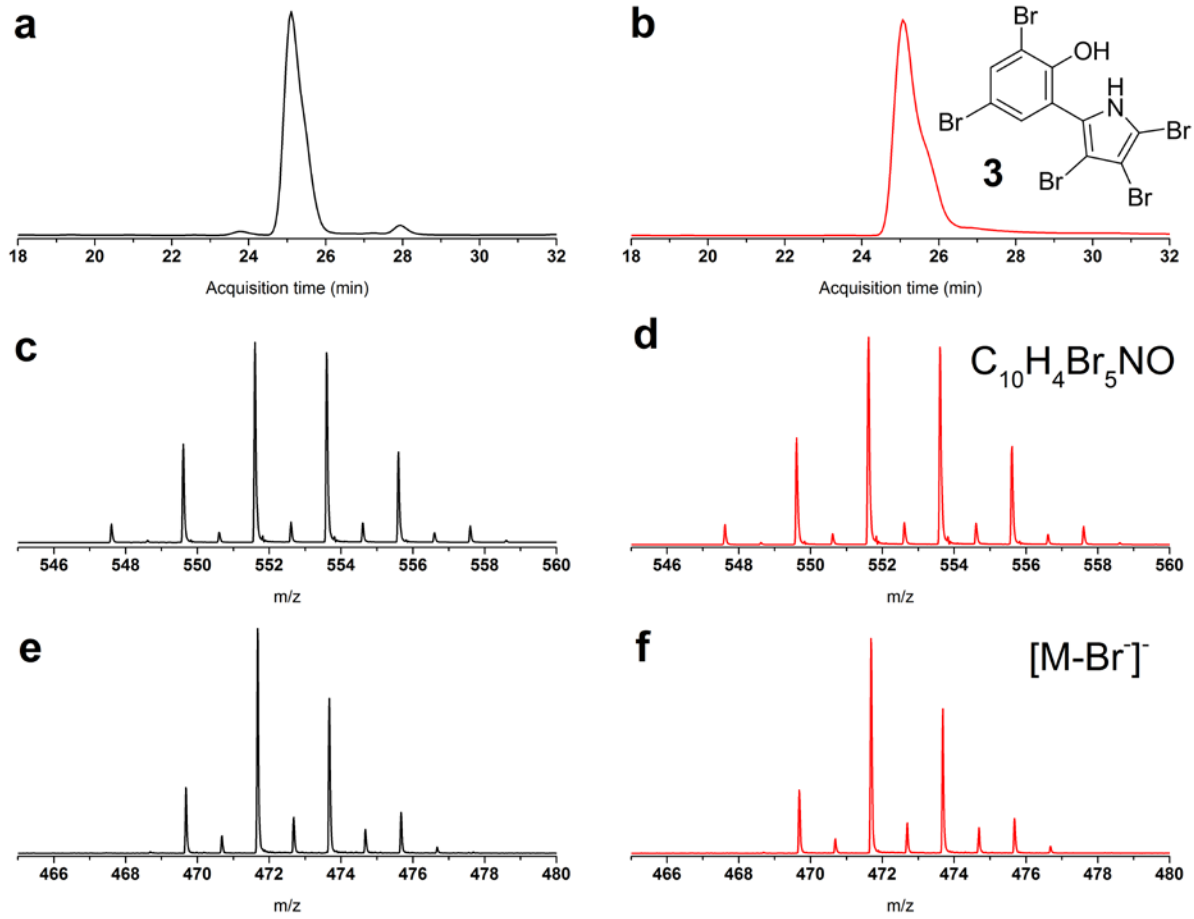

Supplementary Fig. 26. Characterization of 3 generated by Bmp7 in an *in vitro* reaction with 4 and 6 as substrates. Extract of Bmp7 reaction (black curves) was compared to an authentic NMR characterized sample of **3** (red curves) isolated from *P. luteoviolacea* 2ta16. (**a**, **b**) Comparison of retention times. MS1 EIC corresponding to the most abundant isotope for the molecular formula $C_{10}H_4Br_5NO$ (m/z = 551.60, 10 ppm tolerance) for the Bmp7 reaction extract (**a**) and authentic standard of **3** (**b**) analyzed under identical chromatographic conditions. (**c**, **d**) Comparison of MS1 profiles. MS1 mass spectrum for species at retention time 25.2 min from the Bmp7 reaction extract (**c**) and authentic standard of **3** (**d**). (**e**, **f**) Comparison of MS/MS profiles. MS2 profile of the product ions generated from most abundant isotope MS1 ions corresponding to the molecular formula $C_{10}H_3Br_4NO$ at identical retention times from the Bmp7 reaction extract (**e**) and authentic standard of **3** (**f**). Most abundant MS2 ions corresponded to the $[M\text{-}Br^-]^-$. Identical retention times, MS1 and MS/MS profiles as compared to a NMR characterized authentic standard lead to the characterization of the Bmp7 reaction product as **3**.

NMR spectrum for **3** purified from preparative scale cultures of *P. luteoviolacea* 2ta16 and used as authentic standard in panels **b**, **d** and **f** above:

3: ^{1}H NMR: ($CDCl_3$) δ [ppm] 9.54 (bs, 1H), 8.09 (d, *J* = 2.4 Hz, 1H), 7.58 (d, *J* = 2.4 Hz, 1H), 6.10 (bs, 1H)

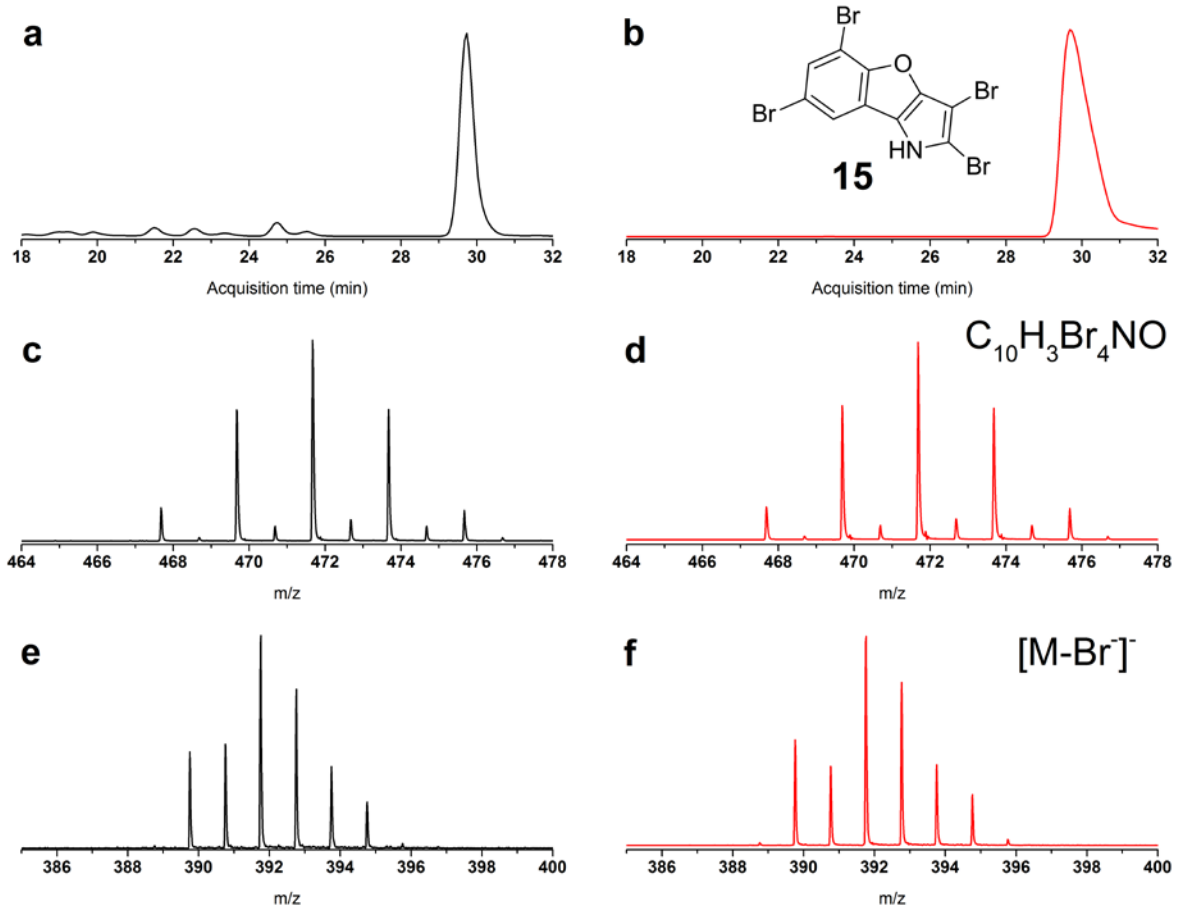

Supplementary Fig. 27. Characterization of 15 generated by Bmp7 in an *in vitro* reaction with 4 and 6 as substrates. Extract of Bmp7 reaction (black curves) was compared to an authentic NMR characterized sample of **15** (red curves) isolated from *P. luteoviolacea* 2ta16. (**a**, **b**) Comparison of retention times. MS1 EIC corresponding to the most abundant isotope for the molecular formula $C_{10}H_3Br_4NO$ (m/z = 471.68, 10 ppm tolerance) for the Bmp7 reaction extract (**a**) and authentic standard of **15** (**b**) analyzed under identical chromatographic conditions. (**c**, **d**) Comparison of MS1 profiles. MS1 mass spectrum for species at retention time 29.8 min from the Bmp7 reaction extract (**c**) and authentic standard of **15** (**d**). (**e**, **f**) Comparison of MS/MS profiles. MS2 profile of the product ions generated from most abundant isotope MS1 ions corresponding to the molecular formula $C_{10}H_3Br_4NO$ at identical retention times from the Bmp7 reaction extract (**e**) and authentic standard of **15** (**f**). Most abundant MS2 ions corresponded to the $[M\text{-}Br^-]^-$. Identical retention times, MS1 and MS/MS profiles as compared to a NMR characterized authentic standard lead to the characterization of the Bmp7 reaction product as **15**.

^{1}H NMR spectrum for **15** purified from preparative scale cultures of *P. luteoviolacea* 2ta16 and used as authentic standard in panels **b**, **d** and **f** above:

15: ^{1}H NMR ($CDCl_3$) δ [ppm] 8.79 (bs, 1H), 7.57 (d, *J* = 1.8 Hz, 1H), 7.54 (d, *J* = 1.8 Hz, 1H)

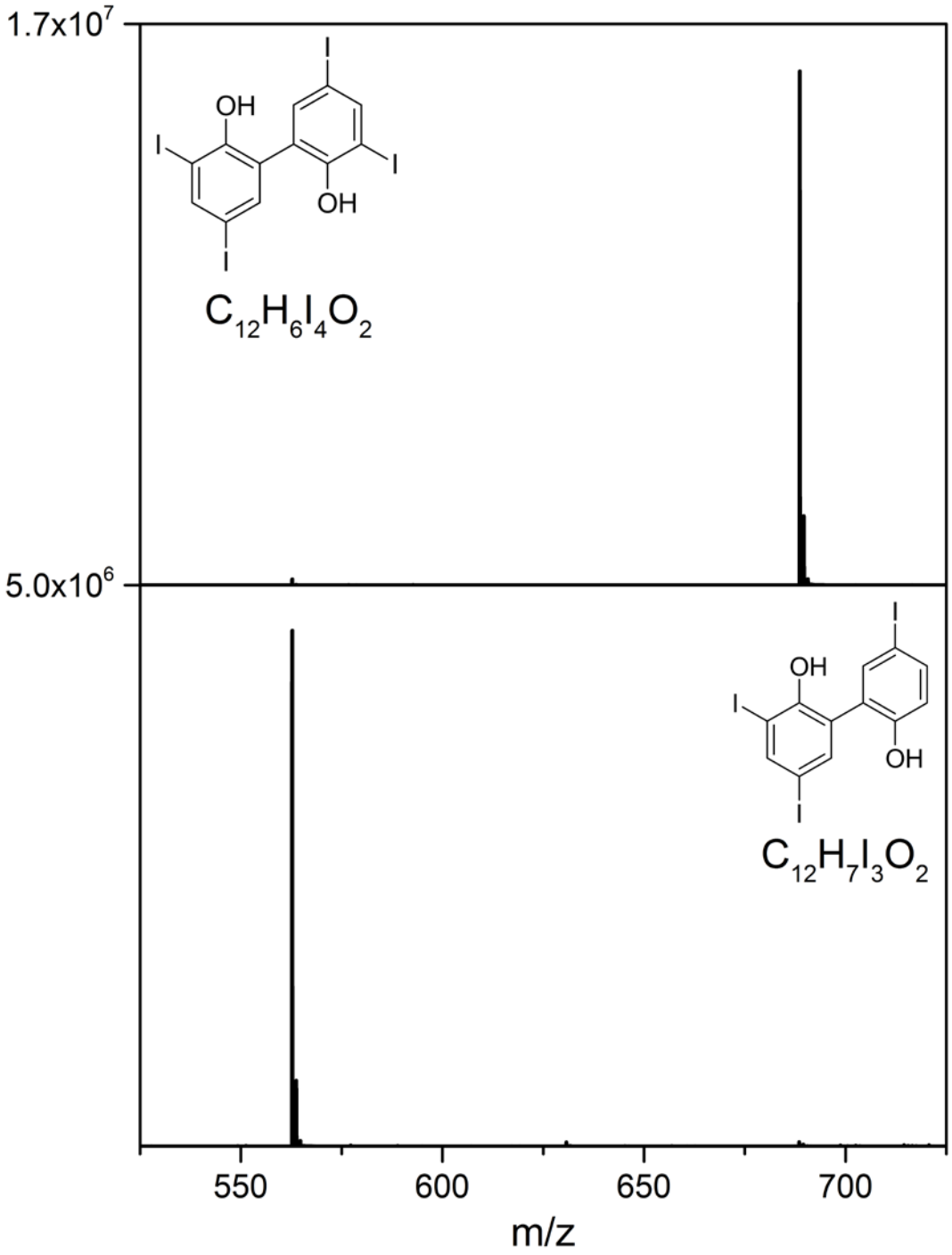

Supplementary Fig. 28. Production of iodinated bromophenols by heterologous host *E. coli* expressing *bmp1–8* grown in the presence of KI. When *E. coli* expressing *bmp1–8* was grown in the presence of 1 g/L KI (no KBr was present), we could detect MS1 signals corresponding to the molecular formulae $C_{12}H_6I_4O_2$ (top) (expected: 688.6474, found: 688.6472) and $C_{12}H_7I_3O_2$ (bottom) (expected: 562.7507, found: 562.7508). The molecular formula $C_{12}H_6I_4O_2$ corresponds to the iodinated analog of **1** (putative structure shown in top

panel), while $C_{12}H_7I_3O_2$ corresponds to the iodinated analog of **10** (putative structure shown in bottom panel). This result implies that Bmp5 could indeed accept iodide for incorporation to 4-HBA. Together with the dimerization of **17** as shown in **Supplementary Fig. 25**, this result demonstrates that Bmp7 is non-specific for the identity of halogens atoms present on the phenol ring to catalyze their coupling. Also note that during this experiment, 10 g/L chloride was present in the *E. coli* growth media. However, we could not detect the formation of any chlorinated phenol monomers or dimers.

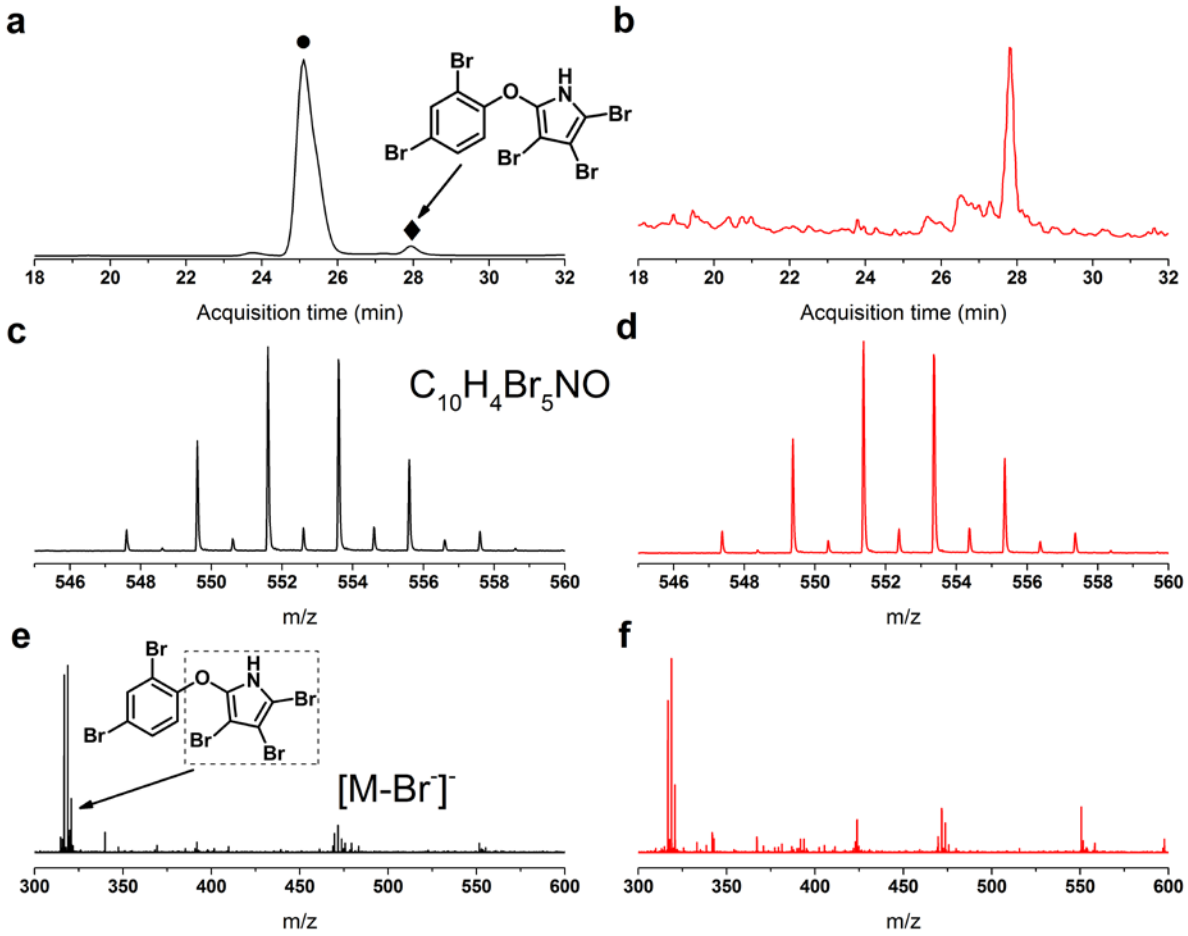

Supplementary Fig. 29. Mass spectrometry based characterization of a polybrominated phenol-pyrrole ether product generated by Bmp7 in an *in vitro* reaction with 4 and 6 as substrates, which is also detected in the culture extracts of *P. luteoviolacea* 2ta16. Extract of Bmp7 reaction (black curves) was compared to an extract of *P. luteoviolacea* 2ta16 (red curves). (**a**, **b**) Comparison of retention times. MS1 EIC corresponding to the most abundant isotope for the molecular formula $C_{10}H_4Br_5NO$ (m/z = 551.60, 10 ppm tolerance) for the Bmp7 reaction extract (**a**) and a MS2 EIC corresponding to m/z = 314.78, 10 ppm tolerance (*vide infra*) for an extract of *P. luteoviolacea* 2ta16 (**b**) analyzed under identical chromatographic conditions. Note that in (**a**), two isomeric molecules corresponding to the molecular formula $C_{10}H_4Br_5NO$ could be detected. Peak denoted by● corresponds to **3**, as shown in **Supplementary Fig. 26**. The peak corresponding to♦ is an isomer of **3**. (**c**, **d**) Comparison of MS1 profiles. MS1 mass spectrum for species at retention time 27.9 min from the Bmp7 reaction extract (**c**) and an extract of *P. luteoviolacea* 2ta16 (**d**). (**e**, **f**) Comparison of MS/MS profiles. MS2 profile of the product ions generated from most abundant isotope MS1 ions corresponding to the molecular formula $C_{10}H_3Br_4NO$ at identical retention times

from the Bmp7 reaction extract (**e**) and an extract of *P. luteoviolacea* 2ta16 (**f**). Most abundant MS2 ions (cluster around m/z = 314.78) corresponded to a hydroxytribromopyrrole moiety (shown in a dashed box in (**e**)), while a $[M-Br]^-$ MS2 product ion can also be detected. Detection of a hydroxytribromopyrrole MS2 ion leads us to postulate that the structure of this molecule could correspond to a polybrominated phenol-pyrrole ether as shown in (**a**).

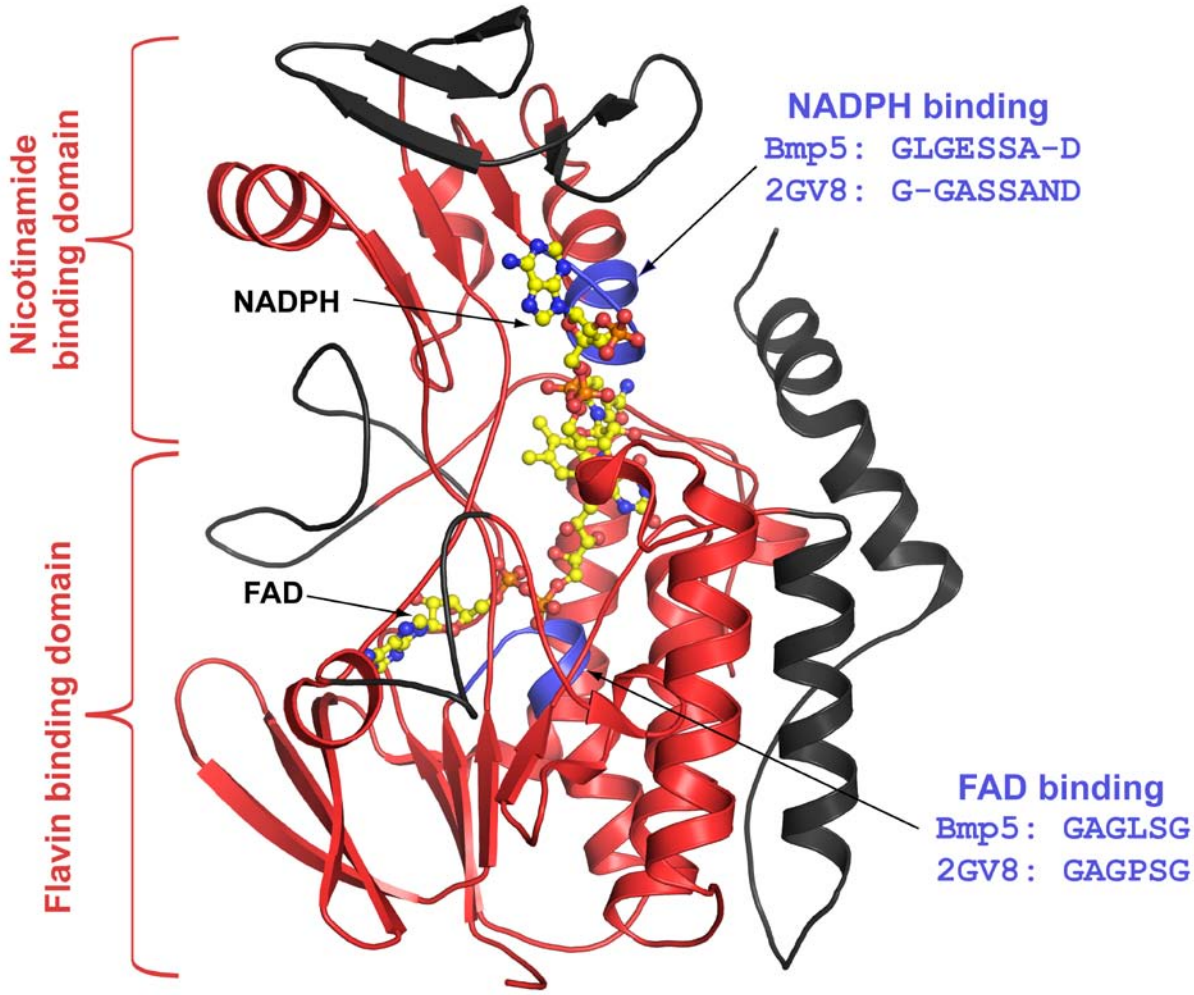

Supplementary Fig. 30. Primary sequence analysis identifies Bmp5 to be homologous to flavin-dependent monooxygenases. Primary sequence of Bmp5 was provided as an input to the NCBI BLAST program and analyzed against the 'Non-reduntant protein sequence (nr)' dataset. All homologs of Bmp5 identified using this analysis (apart *P. phenolica* O-BC30 and *M. mediterranea* MMB-1, as decribed in this study) were annotated as flavin-dependent dimethylaniline monooxygenases. However, as most of the sequences returned by the BLAST search were also annotated as hypothetical or predicted proteins with uncharacterized biochemical activities, a second BLAST search was performed against the 'Protein Data Bank (pdb)' database. The results of this search were more definitive, and are discussed here. The primary structural homologs for Bmp5 that had the most primary sequence coverage identified were:

1. PDB: 2GV8 and related structures. Flavin-dependent monooxygenase from *Schizosaccharomyces pombe*[14].

2. PDB: 2XVI and related structures. Flavin-dependent monooxygenase from *Methylophaga aminisulfidivorans*[15].

Further analysis reveals that the for both 2GV8 and 2XVI, homology to Bmp5 is divided into two distinct regions. The first region comprises of residues from the N-terminus of Bmp5 to residue 200 (identity/similarity = 28%/43% to 2GV8 and 27%/48% to 2XVI; henceforth referred to as *Motif 1*). The second region comprises of residues 315 to 426 (identity/similarity = 25%/47% to 2GV8 and 29%/46% to 2XVI; henceforth referred to as *Motif 2*). Upon mapping both regions back on to the structure 2GV8 (shown in cartoon representation above), it is evident that *Motif 1* and *Motif 2* (colored red in cartoon representation) comprise of all core secondary structural elements constututing the flavin binding and the nicotinamide binding domains. This includes the flavin binding GAGLSG sequence motif (colored blue), and the nicotinamide binding GLGESSAD sequence motif[14-15] (colored blue) identified in the primary sequence of Bmp5. Hence, the core structural elements in the structure of 2GV8 for both flavin binding, as well as nicotinamide binding can be identified in the primary sequence for Bmp5.

It is also noteworthy that the BLAST search for the primary sequence of Bmp5 against the PDB database did not return any hits for flavin-dependent halogenases, either of the PrnA[16]/RebH[17]/PyrH[18] (and an unpublished crystal structure PDB: 2PYX) type that utilize free substrates, or of the CmlS[19]/CndH[20] type that utilize substrates tethered to acyl carrier proteins. On the flip side, an identical BLAST search against the PDB database for the primary sequence of Bmp2 returns homology to CndH (31%/47%), CmlS (30%/45%) and an unpublished crystal structure PDB: 3NIX (28%/44%). A similar result is obtained for the following halogenases: chlorinase PltA[1] (CmlS: 30%/45%; CndH: 28%/46%; 3NIX: 27%/45%), chlorinase SgcC3[21] (CmlS: 36%/52%; CndH: 53%/66%; 3NIX: 32%/44%), chlorinase Mpy16[22] (CmlS: 30%/43%; CndH: 32%/49%; 3NIX: 26%/44%), chlorinase Clz5[23] (CmlS: 30%/43%; CndH: 32%/49%; 3NIX: 26%/44%), chlorinase Pyr29[24] (CmlS: 31%/45%; CndH: 30%/47%; 3NIX: 28%/44%), among other flavin-dependent halogenases that have been described in literature. Noteworthy here is the chlorinase ChlA[25]. Activity for ChlA was demonstrated for a substrate molecule not tetherred to an ACP molecule. However, ChlA demonstrates greatest homology to halogenases requiring ACP tethered substrates (CmlS: 25%/40%; CndH: 20%/38%; 3NIX was not returned as a homolog by BLAST). Expectedly, tryptophan chlorinases KtzQ and KtzR[26] display homology to PrnA/RebH/PyrH.

Supplementary Tables

Supplementary Table 1. High-resolution MS used for determination of molecular formulae of polybrominated metabolites from extract of *P. luteoviolacea* 2ta16.

Molecule	Molecular Formula	$[M-H]^-$ calculated (m/z)	$[M-H]^-$ measured (m/z)	Error (mmu)
1	$C_{12}H_6Br_4O_2$	496.7029	496.7029	0.0
2	$C_8H_2Br_6N_2$	598.5245	598.5244	0.1
3	$C_{10}H_4Br_5NO$	547.6137	547.6137	0.0
4	$C_6H_4Br_2O$	248.8556	248.8554	0.2
5	$C_6H_3Br_3O$	326.7661	326.7660	0.1
6	$C_4H_2Br_3N$	299.7665	299.7663	0.2
7	C_4HBr_4N	377.6770	377.6765	0.5
9	$C_{12}H_7Br_3O_2$	418.7923	418.7922	0.1
14	$C_{10}H_3Br_4NO$	467.6875	467.6874	0.1

Supplementary Table 2. *P. luteoviolacea* 2ta16 *bmp* gene cluster annotation.

Gene	Locus tag	Size [aa]	Proposed function	Homolog (%Similarity/%Identity) *functionally characterized	Accession number
bmp1	*Pl2ta16_01235*	77 (1–77)	Prolyl acyl carrier protein (N-terminal domain)	PltL, peptidyl carrier protein [*Pseudomonas protegens* pf-5] (60/34)*	YP_259898.1
bmp1	*Pl2ta16_01235*	280 (78–358)	Thioesterase (C-terminal domain)	α/β-hydrolase fold protein [*Krypidia tusciae* DSM 2912] (47/28)	YP_003588846
bmp2	*Pl2ta16_01236*	406	Pyrrole halogenase	PltA, $FADH_2$-dependent halogenase [*Pseudomonas protegens* Pf-5] (44/29)*	AAY92059.1
bmp3	*Pl2ta16_01237*	380	Proline dehydrogenase	PltE, acyl-CoA dehydrogenase [*Pseudomonas protegens* Pf-5] (62/45)*	AAY92063.1
bmp4	*Pl2ta16_01238*	518	L-Proline adenyl transferase	PltF, prolyl-AMP ligase [*Pseudomonas protegens* pf-5] (55/40)*	YP_259898.1
bmp5	*Pl2ta16_01239*	515	Flavin-dependent oxygenase	Dimethylaniline monooxygenase (N-Oxide forming) [*Myotis brandtii*] (50/33)	EPQ08634.1
bmp6	*Pl2ta16_01240*	202	Chorismate lyase	4-hydroxybenzoate synthetase [*Beggiatoa alba*] (60/41)	WP_002683800.1
bmp7	*Pl2ta16_01241*	491	Cytochrome P450	Cytochrome P450 [*Phalacrocorax carbo*] (50/30)	BAE93469.1
bmp8	*Pl2ta16_01234*	196	Carboxymuconolactone decarboxylase	Carboxymuconolactone decarboxylase [*Blastococcus saxobsidens* DD2] (58/42)	YP_005328578.1
bmp9	*Pl2ta16_01233*	106	Ferredoxin	Ferredoxin [*Idiomarina loihiensis* L2TR] (73/52)	YP_155277.1
bmp10	*Pl2ta16_01232*	415	Ferredoxin reductase	Ferredoxin reductase [*Pseudomonas* sp. 19-rlim] (70/53)	AEO27387.1

Supplementary Table 3. Primers used to generate overlapping fragments for yeast assembly of yeast/*E. coli* shuttle vector pGAL-*bmp1–7*. All primer sequences are listed from 5' to 3'.

Primer Name	Primer Sequence	Target
pGALbmp1F	AAGGTAAACAGGTAAGAGCTCGGTAATAACTG ATATAATTAAATTGAAG	pGAL-MF region1
pGALbmp1F	TGCAGTCTCTTGATAACTTTTTGCACTGTAGGTC CGTTAA	pGAL-MF region1
pGALbmp2F	TTAACGGACCTACAGTGCAAAAAGTTATCAAGA GACTGCA	pGAL-MF region2
pGALbmp2F	CTAGTCTGGCAATATTGTTAACACTAGTGACTC GCTGCGCTCGGTC	pGAL-MF region2
pGALbmp3F	ACCGAGCGCAGCGAGTCACTAGTGTTAACAATA TTGCCAGACTAGA	*bmp* cluster region1
pGALbmp3F	TTGGCCCAGGTAACCGAATTTAGCATTCGTAGT GGCATAC	*bmp* cluster region1
pGALbmp4F	GTATGCCACTACGAATGCTAAATTCGGTTACCT GGGCCAA	*bmp* cluster region2
pGALbmp4F	TGTGATCTTGTACTCAGTTTGCCAATGTTTCGTA TCGTAC	*bmp* cluster region2
pGALbmp5F	GTACGATACGAAACATTGGCAAACTGAGTACA AGATCACA	*bmp* cluster region3
pGALbmp5F	AATTTAATTATATCAGTTATTACCGAGCTCTTAC CTGTTTACCTTCGGGT	*bmp* cluster region3

Supplementary Table 4. Primers used to generate gene deletions from pETDuet-*bmp*. All primer sequences are listed from 5' to 3'.

Primer Name	Primer Sequence	ORF deleted
bmp2KO FWD	CATGGCATGAAGGAAAAGCACTGCGCTTTTCCTTCT AAGGGAAGGATTGATTATG	*bmp2*
bmp2KO REV	TGCTTTTCCTTCATGCCATGTCCACCTTAGTTAAGA AGTCTTCAACAACCCAGAC	
bmp5KO FWD	TGGTGCGTAAATAGTACGAGAAAGGACATGATTCG ATTGTCAGATGAAAGCCTGT	*bmp5*
bmp5KO REV	CTCGTACTATTTACGCACCACTTTGCACAGTATTAC TCCCGTGCCGTGGGCGAGT	
bmp7-XmaF	ACACCAGAATTATCAACCTTAGTCAGTGGGATTTG ACCACCCGGGGCTCACGGTAACTGATGCCG	*bmp7*
bmp7-XmaR	TAAGGATGGATGCAAAACCATCCTAAGTAGGATGG CCTTCCCGGGGGAACTTATGAGCTCAGCCA	

Supplementary Table 5. Co-transformations of *E. coli* BL21(DE3) for heterologous expression of *bmp* cluster and derivatives.

Strain name	Co-transformed plasmid 1	Co-transformed plasmid 2
bmp1–8	pETDuet-*bmp1–7*	pCOLADuet-*bmp8-ppt*
Δbmp2	pETDuet-*bmp1–7:Δbmp2*	pCOLADuet-*bmp8-ppt*
Δbmp5	pETDuet-*bmp1–7:Δbmp5*	pCOLADuet-*bmp8-ppt*
Δbmp7	pETDuet-*bmp1–7:Δbmp7*	pCOLADuet-*bmp8-ppt*
Δbmp8	pETDuet-*bmp1–7*	pCOLADuet-*ppt*

SUPPLEMENTARY REFERENCES

1 Dorrestein, P. C., Yeh, E., Garneau-Tsodikova, S., Kelleher, N. L. & Walsh, C. T. Dichlorination of a pyrrolyl-S-carrier protein by FADH2-dependent halogenase PltA during pyoluteorin biosynthesis. *Proc Natl Acad Sci U S A.* **102**, 13843-13848 (2005).

2 Dorrestein, P. C. *et al.* Facile detection of acyl and peptidyl intermediates on thiotemplate carrier domains via phosphopantetheinyl elimination reactions during tandem mass spectrometry. *Biochemistry.* **45**, 12756-12766 (2006).

3 Isnansetyo, A. & Kamei, Y. MC21-A, a bactericidal antibiotic produced by a new marine bacterium, *Pseudoalteromonas phenolica* sp. nov. O-BC30(T), against methicillin-resistant *Staphylococcus aureus*. *Antimicrob Agents Chemother.* **47**, 480-488 (2003).

4 Feher, D., Barlow, R., McAtee, J. & Hemscheidt, T. K. Highly brominated antimicrobial metabolites from a marine *Pseudoalteromonas* sp. *J Nat Prod.* **73**, 1963-1966 (2010).

5 Belin, P. *et al.* Identification and structural basis of the reaction catalyzed by CYP121, an essential cytochrome P450 in *Mycobacterium tuberculosis*. *Proc Natl Acad Sci U S A.* **106**, 7426-7431 (2009).

6 Zhao, B. *et al.* Binding of two flaviolin substrate molecules, oxidative coupling, and crystal structure of *Streptomyces coelicolor* A3(2) cytochrome P450 158A2. *J Biol Chem.* **280**, 11599-11607 (2005).

7 Dec, J., Haider, K. & Bollag, J. M. Release of substituents from phenolic compounds during oxidative coupling reactions. *Chemosphere.* **52**, 549-556 (2003).

8 Mas, S. *et al.* Comprehensive liquid chromatography-ion-spray tandem mass spectrometry method for the identification and quantification of eight hydroxylated brominated diphenyl ethers in environmental matrices. *J Mass Spectrom.* **42**, 890-899 (2007).

9 Li, D. B. *et al.* Chapter 19. In vitro studies of phenol coupling enzymes involved in vancomycin biosynthesis. *Methods Enzymol.* **458**, 487-509 (2009).

10 John, E. A., Pollet, P., Gelbaum, L. & Kubanek, J. Regioselective syntheses of 2,3,4-tribromopyrrole and 2,3,5-tribromopyrrole. *J Nat Prod.* **67**, 1929-1931 (2004).

11 Petersen, B. O. *et al.* H2BC: a new technique for NMR analysis of complex carbohydrates. *Carbohydr Res.* **341**, 550-556 (2006).

12 Calcul, L. *et al.* NMR strategy for unraveling structures of bioactive sponge-derived oxy-polyhalogenated diphenyl ethers. *J Nat Prod.* **72**, 443-449 (2009).

13 Kitamura, M., Koyama, T., Nakano, Y. & Uemura, D. Corallinafuran and Corallinaether, novel toxic compounds from crustose coralline red algae. *Chemistry Letters.* **34**, 1272-1273 (2005).

14 Eswaramoorthy, S., Bonanno, J. B., Burley, S. K. & Swaminathan, S. Mechanism of action of a flavin-containing monooxygenase. *Proc Natl Acad Sci U S A.* **103**, 9832-9837 (2006).

15 Cho, H. J. *et al.* Structural and functional analysis of bacterial flavin-containing monooxygenase reveals its ping-pong-type reaction mechanism. *J Struct Biol.* **175**, 39-48 (2011).

16 Dong, C. *et al.* Tryptophan 7-halogenase (PrnA) structure suggests a mechanism for regioselective chlorination. *Science.* **309**, 2216-2219 (2005).

17 Bitto, E. *et al.* The structure of flavin-dependent tryptophan 7-halogenase RebH. *Proteins.* **70**, 289-293 (2008).

18 Zhu, X. *et al.* Structural insights into regioselectivity in the enzymatic chlorination of tryptophan. *J Mol Biol.* **391**, 74-85 (2009).

19 Podzelinska, K. *et al.* Chloramphenicol biosynthesis: the structure of CmlS, a flavin-dependent halogenase showing a covalent flavin-aspartate bond. *J Mol Biol.* **397**, 316-331 (2010).

20 Buedenbender, S., Rachid, S., Muller, R. & Schulz, G. E. Structure and action of the myxobacterial chondrochloren halogenase CndH: a new variant of FAD-dependent halogenases. *J Mol Biol.* **385**, 520-530 (2009).

21 Lin, S., Van Lanen, S. G. & Shen, B. Regiospecific chlorination of (S)-beta-tyrosyl-S-carrier protein catalyzed by SgcC3 in the biosynthesis of the enediyne antitumor antibiotic C-1027. *J Am Chem Soc.* **129**, 12432-12438 (2007).

22 Yamanaka, K., Ryan, K. S., Gulder, T. A., Hughes, C. C. & Moore, B. S. Flavoenzyme-catalyzed atropo-selective N,C-bipyrrole homocoupling in marinopyrrole biosynthesis. *J Am Chem Soc.* **134**, 12434-12437 (2012).

23 Mantovani, S. M. & Moore, B. S. Flavin-linked oxidase catalyzes pyrrolizine formation of dichloropyrrole-containing polyketide extender unit in chlorizidine A. *J Am Chem Soc.* **135**, 18032-18035 (2013).

24 Zhang, X. & Parry, R. J. Cloning and characterization of the pyrrolomycin biosynthetic gene clusters from *Actinosporangium vitaminophilum* ATCC 31673 and *Streptomyces* sp. strain UC 11065. *Antimicrob Agents Chemother.* **51**, 946-957 (2007).

25 Neumann, C. S., Walsh, C. T. & Kay, R. R. A flavin-dependent halogenase catalyzes the chlorination step in the biosynthesis of *Dictyostelium* differentiation-inducing factor 1. *Proc Natl Acad Sci U S A.* **107**, 5798-5803 (2010).

26 Fujimori, D. G. *et al.* Cloning and characterization of the biosynthetic gene cluster for kutznerides. *Proc Natl Acad Sci U S A.* **104**, 16498-16503 (2007).

27 Thomas, M. G., Burkart, M. D. & Walsh, C. T. Conversion of L-proline to pyrrolyl-2-carboxyl-S-PCP during undecylprodigiosin and pyoluteorin biosynthesis. *Chem Biol.* **9**, 171-184 (2002).